Feasibility of a Radially Cooled Thorium Breeder Pebble Bed type High Temperature Reactor

Master Thesis

Joran de Jong

26/06/2014

TU Delft Delft University of Technology

Challenge the future

FEASIBILITY OF A RADIALLY COOLED THORIUM BREEDER PEBBLE BED TYPE HIGH TEMPERATURE REACTOR

by

Joran de Jong

in partial fulfillment of the requirements for the degree of

Master of Science
in Applied Physics

at the Delft University of Technology,
to be defended publicly on Friday July 4, 2014 at 2:00 PM.

Supervisors:	Dr. J. L. Kloosterman,
	Ir. F. J. Wols.
Thesis committee:	Dr. J. L. Kloosterman,
	Dr. S. Kenjeres,
	Dr. D. Lathouwers,
	Ir. F. J. Wols.

TU Delft Delft University of Technology

REACTOR INSTITUTE DELFT

ABSTRACT

The world demand on energy, combined with environmental concerns, constitutes the need for a plentiful supply of safely produced energy without carbon emissions. The High Temperature Reactor (HTR) is the predecessor of the Gen-4 VHTR design, and has a large thermal efficiency and unsurpassed safety features. Thorium offers more natural resources, more proliferation resistance, and better waste characteristics than uranium. The safety features of the HTR and the resourcefulness of thorium can be combined in a thorium breeder pebble bed reactor.

In this research, radial cooling is proposed as an improvement to this reactor type, specifically to solve or strongly mitigate the problems involved with the high pressure drop, temperature variations and reactivity control. The system was compared to the axially cooled case to investigate the effects of the change in coolant direction, and studies have been performed to research the physical feasibility of radial cooling within practical and safety constraints.

MATLAB models were built to compare the thermal hydraulic behaviour of axially and radially cooled core designs. In order to verify the thermal hydraulics and include neutronics in the simulation, the feasibility of the radially cooled core was investigated in more detail using coupled THERMIX / DALTON steady state calculations. Transient behaviour was researched with THERMIX in stand alone mode.

It was found that radial cooling is a feasible design option for this reactor type. The placement of a central reflector allows sufficient regulation of the mass flow distribution, leading to small helium outflow temperature variations. The control rods can be placed in the central reflector, especially for the system with outward cooling, where the rods are constantly cooled by fresh helium. The pressure drop was found to decrease from 1.2 bar to 38 millibar.

Simulations on both pressurized as well as depressurized loss of forced cooling incidents with SCRAM have been performed, and the maximum temperature remains well under 1600°C in both these cases. Reversing the coolant flow direction to inward cooling enhances the radial spread in power density, which lowers the maximum transient temperatures. However, it has a negative effect on reactivity and makes the placement of the reactivity control system in the central reflector more troublesome due to the higher centre core temperature. This means that the system with outward radial cooling is considered more favourable.

NOMENCLATURE

Symbol	*Unit*	*Description*
A	m^2	Cross sectional area
A_{spheres}	m^2	Combined surface area of the spheres
A_{sphere}	m^2	Surface area of one sphere
A_{slits}	m^2	Combined cross sectional area of the slits
A_{tot}	m^2	Total surface area of the reflector
c_p	J/K	Heat capacity
D	m	Bed diameter
D	cm^2/s	Diffusion coefficient
d_{h}	m	Hydraulic diameter
d_{p}	m	Pebble diameter
$\boldsymbol{F}$	cm^{-1}	Neutron production operator
f	-	Friction factor that depends on the Reynolds number
f_{area}	-	Surface area fraction occupied by flow paths
$f_{z,E}$	-	flux disadvantage factor
H	m	Height of the bed
$\boldsymbol{J}$	$cm^{-2}s^{-1}$	Neutron current
k	-	Multiplication factor
$K_{\text{ax/ra}}$	-	Axial/radial parametric constant
k_{eff}	-	Effective multiplication factor
L	m	Length
l_{mfp}	m	Mean free path length
$\boldsymbol{M}$	cm^{-1}	Neutron destruction operator
$\dot{m}$	kg/s	Mass flow rate
$\dot{M}$	kg/s	Total mass flow rate
Nu_r	-	Radiative Nusselt number
p	Pa	Pressure
Δp	Pa	Pressure drop
P_{w}	m	Wetted Perimeter
P_p	J/s	Pumping power
Pe	-	Peclet number
q_c'''	W/m^3	Convective heat source
q_n'''	W/m^3	Nuclear power density
R	J/kg/K	Universal gas constant
Re	-	Reynolds number
T	K	Temperature
t	s	Time
T_{in}	K	Coolant inflow temperature
T_{out}	K	Coolant outflow temperature
v	m/s	Coolant velocity
V_{bed}	m^3	Volume of the bed
v_{p}	m/s	Mean velocity of the coolant between the pebbles
V_{spheres}	m^3	Combined volume of the spheres
v_g	m/s	Speed of a neutron in energy group g
V_z	m^3	Zone Volume
X_G	eV	Quantity X for neutrons in broad energy group G
X_g	eV	Quantity X for neutrons in fine meshed energy group G

Symbol	*Unit*	*Description*
α	$W/m^2/K$	Heat transfer coefficient
ϵ	-	Void fraction (porosity)
ϵ_r	-	Radiative emissivity coefficient
ζ	m	Root mean square roughness of a surface
λ	J/m/K/s	Effective conductivity
$\lambda_{\text{ax/ra}}$	W/m/K	Axial/Radial effective conductivity
λ_{fs}	W/m/K	Solid layer to layer conductive and radiative heat conductivity
λ_{g}	W/m/K	Coolant gas conductivity
λ_{gap}	W/m/K	Equivalent gap conductivity for heat conduction and radiation
λ_{o}	W/m/K	Conductive and radiative heat conductivity
λ_{solid}	J/m/K/s	Solid graphite conductivity
μ	Pa s	Dynamic viscosity
$\bar{\mu}_0$	-	Average scatter angle cosine
ν	#	Number of neutrons generated in a fission event
ρ	kg/m^3	Density of the coolant
ρ_{solid}	kg/m^3	Density of the graphite
σ	$J\,s^{-1}m^{-2}K^{-4}$	Stefan-Boltzmann constant
σ_x	cm^2	Microscopic cross section for reaction x
Σ_x	cm^{-1}	Macroscopic cross section for reaction x
ϕ	$cm^{-2}s^{-1}eV^{-1}$	Energy dependent neutron flux
$\vec{\phi}$	$cm^{-2}s^{-1}$	Vector flux
$\vec{\phi}_0$	$cm^{-2}s^{-1}$	Initial vector flux guess
χ_g	-	Chance that a fission neutron is born in energy group g
ψ	-	Pressure drop coefficient
$\hat{\Omega}$	-	Unit direction

Acronym	*Description*
AVR	Arbeitsgemeinschaft VersuchsReaktor
CFD	Computational Fluid Dynamics
CSAS	Critical Safety Analysis Sequence
DLOFC	Depressurized Loss Of Forced Cooling
HTR	High Temperature Reactor
HTR-10	Experimental 10 MW High Temperature Reactor
HTR-PM	High Temperature Reactor - Pebble bed Modular
HTTR	High Temperature Test Reactor
ICE	Intermix Cross sections Effortlessly
LOFC	Loss Of Forced Cooling
LWR	Light Water Reactor
MA	Minor Actinides
PBMR	Pebble Bed Modular Reactor
PLOFC	Pressurized Loss Of Forced Cooling
PyC	Pyrolytic Carbon
RHRS	Residual Heat Removal System
RPV	Reactor Pressure Vessel
SiC	Sillicon Carbide
THTR	Thorium High Temperature Reactor
TRISO	TRistructural-ISOtropic
VHTR	Very High Temperature Reactor

CONTENTS

1

INTRODUCTION

1.1. NUCLEAR POWER GENERATION

WORLD DEMAND ON ENERGY

The amount of energy consumed has risen sharply over the past centuries. The demand continues to grow and is estimated to increase by fifty percent between now and the year 2030. This increasing demand is not only due to the ever-expanding world population, but also due to the increase in average energy consumption per capita. Especially in the near future this factor will have a strong influence, as large countries like China, India and Brazil reach an economic level where access to electric power suddenly comes into reach for the majority of the population. Besides this increasing growth in energy demand, the concerns about climate change and the inevitable exhaustion of traditional fossil fuels effect a need for alternatives with sufficient resources and low carbon emissions.

CURRENT STATE OF NUCLEAR POWER

Nuclear energy can contribute substantially to a more sustainable global energy production. However, it has its drawbacks, the most important of which is the risk of accidents. Nuclear power production inevitably leads to the production of radioactive waste. This makes the consequences of an accident in a nuclear power plant much more serious than those of an accident in any other type of power facility. Further, the thermal efficiency of current nuclear reactors is low compared to traditional power plants, the amount of easily minable uranium-235 is limited and the radioactive waste needs to be stored in deep geological repositories. Hence, although nuclear power does not cause the massive carbon dioxide pollution of fossil fuels such as coal and oil, it cannot be called fully sustainable. Besides these technical issues, a negative public perception results in nuclear energy being regarded as a less favorable source of energy. Fortunately, the current design of nuclear reactors is not the endpoint of nuclear engineering. Major improvements are theoretically possible, and might be feasible for commercial application.

GENERATION IV INITIATIVE

Recently, nine of the countries with large nuclear industries founded the Generation IV International Forum, a framework for international cooperation in research and development for the next generation of nuclear energy systems. In the generation IV initiative, six innovative reactor designs were selected for being the most promising advanced nuclear energy systems. These reactors feature enhanced performance in the areas of safety, optimal use of resources, economics, proliferation resistance, and waste reduction. One of these innovative reactor designs is called the Very High Temperature Reactor (VHTR). Its predecessor is a similar system that operates under slightly lower temperatures, and is called the High Temperature Reactor (HTR).

1.2. HIGH TEMPERATURE REACTORS

TECHNOLOGICAL CONCEPT

The High Temperature Reactor, or HTR, has a core that consists of a graphite moderator, and is cooled by helium. These types of reactors are characterized by two distinct geometries for the graphite in the core. The first one is the prismatic block type. Here, the graphite containing the fissionable material is shaped in large blocks with cylindrical holes for the coolant flow. Examples of this type of reactor are the experimental Dragon reactor in de UK, Peach Bottom in the USA and the HTTR in Japan [1]. The second geometry is the pebble bed type. In this type, the fuel is contained in a spherical graphite matrix, surrounded by an extra layer of graphite, forming a "ball" of about 6 cm in diameter. These so-called pebbles are stacked in a cylindrical or annular reactor vessel. The resulting randomly packed stack is referred to as the pebble bed. Coolant can flow through the space between the pebbles, as the random packing of spheres has a porosity (open volume fraction) of about 39 percent. Higher packing fractions can be reached for an orderly packed bed [2]. However, the practical concerns related with orderly stacking a pebble bed reactor make that it is not considered as an option in this research. Examples of pebble bed reactors are the experimental AVR reactor and the commercial THTR-300 in Germany, both of which were partially fueled by thorium. More recently, HTR technology is being developed in China, in the experimental HTR-10 facility, and the scheduled HTR-PM [3].

COATED PARTICLE FUEL

The fuel form that is used in HTRs is called coated particle fuel. Inside the graphite matrix there are thousands of small (/ 1mm) micro spheres , that consist of a fuel kernel surrounded by several protective (ceramic) layers (Fig. 1.1). This type of fuel is called coated particle fuel. The concept of ceramic coated particle fuels was already developed in the late 50's [1]. However, coated particle fuel was not economically competitive, due to the lack of efficient production techniques, and the already full-scale use of fuel in the form of the more traditional Light Water Reactor (LWR) fuel pellets. Hence the concept was abandoned for several decades. Nowadays, the need for safe and sustainable nuclear power, and the improved technological abilities have sparked a new interest in coated particle fuels. The most widely used coated particle is the tristructural-isotropic (TRISO) fuel. It consists of a fuel kernel (usually UO2, but it can also be ThO2, or other fuels) surrounded by four protective layers. The first layer is a porous carbon buffer, that accommodates swelling of the kernel and provides space for gaseous fission product accumulation. This layer is followed by a pyrolytic carbon (PyC) layer, that formes a first boundary to (especially gaseous) fission products and acts as pressure vessel for the kernel. The third layer consists of silicon carbide (SiC). This layer provides a strong diffusion barrier to prevent the release of fission products. The final layer is again a pyrolytic carbon layer, which protects the microspheres and mitigates outside stresses. TRISO fuel particles are designed to retain their fission products, and keep their structural integrity, for temperatures up to 1600°C.

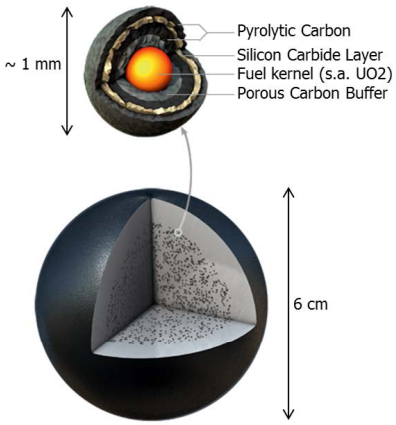

Figure 1.1: Pebble containing fuel kernels with coating layers

SAFETY FEATURES

High temperature reactor fuel can safely sustain temperatures up to 1600°C [4]. Most of the reactors currently in use are LWRs, which can only sustain temperatures up to about 700°C. Due to the difference in allowed operating temperature, the thermal efficiency of a HTR can be much higher than

that of a LWR (45% in stead of 35% [3]). The thermal efficiency could theoretically be raised even further by adopting the direct Brayton cycle for the energy conversion [5]. Yet this is not the main advantage of this reactor type. The combination of the high maximum allowed fuel temperature with the excellent thermal conductivity of graphite and a sleek core design, means that cooling by merely passive mechanisms is very efficient. In the event of an incident where the reactor experiences a loss of forced cooling, passive mechanisms such as conduction, radiation and sometimes natural convection are enough to carry off the decay heat, preventing the core from overheating [6]. No active reactor heat removal systems are needed to maintain the structural integrity of the reactor core and prevent radiological release. That makes this type of reactor inherently safe. Due to the low neutron absorbtion rate of graphite and helium, this reactor type could also utilize thorium as a nuclear fuel, which will be explained in further detail in the next section.

1.3. THORIUM AS A NUCLEAR RESOURCE

BREEDING PROCESS

Instead of the more traditional uranium fuel, thorium too can be used as a resource for nuclear power generation. Thorium is a heavy metal that is just slightly lighter than uranium. Unlike uranium, thorium is not a fissile material in itself. It is a fertile material, which means that it transmutes to a fissile material after absorbing a neutron. This is what is known as the converting process [7]. This process starts when a ^{232}Th nucleus captures a neutron. The resulting ^{233}Th is unstable with a half life of approximately 22 minutes, and decays to ^{233}Pa. This isotope of protactinium will decay with a half life of roughly 27 days to the fissile isotope ^{233}U. This uranium isotope has better neutronic properties than ^{235}U, like a higher fission/absorption ratio in a very large energy region. An important point is that per fission, two neutron absorptions are needed to reach effective breeding: one for the breeding and another for the fissioning itself. This in contrast to using traditional uranium fuels, where only the fission-initiating neutron is required. Fission only generates two and a half neutrons on average, hence the neutron losses in a thorium breeder reactor have to be much lower than in a uranium-fueled reactor.

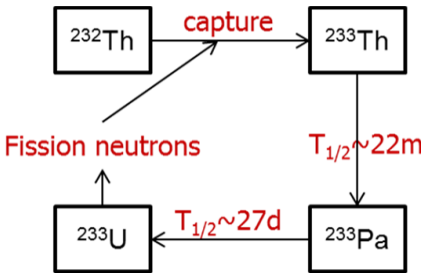

Figure 1.2: The process of converting ^{232}Thorium into ^{233}Uranium

ADVANTAGES

Using thorium as a nuclear resource has lots of advantages over the traditional uranium fuel cycle. First, there is its abundance. Thorium is 3 to 4 times more abundant than uranium in the earth's crust, and it only occurs in one isotope hence it is completely usable. This unlike uranium, where the fraction of fissile material is only 0.7 percent, and hence enrichment of the raw material is usually necessary. Furthermore, the mining and extraction of thorium from its most common ores is relatively easy [8]. This can make thorium a cost effective nuclear resource that could sustain our complete electrical energy usage for thousands of years.

The second large advantage is the waste type resulting from use of thorium instead of uranium in a power plant. The main sources of radioactivity in nuclear waste are the fission products. These are inherent to the process of generating power by nuclear fission, and their production cannot be avoided, no matter what fuel cycle. However, the elements that are specifically responsible for the long-lived radioactivity of nuclear waste are plutonium and the so-called minor actinides (MA). MA comprises all actinide elements besides uranium and plutonium. Of major concern with respect to long lived radiotoxicity are the various americium isotopes. These heavy elements are created in the

traditional uranium fuel cycle by neutron absorption of ^{238}U, and further activation of the resulting ^{239}Pu. As this uranium isotope is inherently present in traditional uranium fuel, the production of these elements is inevitable. In the thorium fuel cycle however, this uranium isotope is not present. Besides, the isotopes that are present are much lighter. Hence, before subsequent activations by neutrons make them reach the heavy Pu and MA, they have to pass ^{233}U and ^{235}U. Both these uranium isotopes are likely to fission under neutron absorbtion, decreasing the amount of Pu and MA substantially [7]. This means that the quantity of long lived waste resulting from the use of thorium as a fuel is far less than that produced using uranium.

Finally, the fact that thorium is not fissile itself makes the raw resource completely proliferation resistant. There are some concerns about the reprocessing and recycling of the bred ^{233}U, which is fissile and could in principle be extracted from the fuel. In the process of breeding ^{233}U from ^{232}Th however, traces of ^{232}U are inevitable. This isotope decays under emission of high energetic gamma rays, making the handling of this type of uranium very difficult, and providing an adequate barrier against proliferation. Obtaining handleable ^{233}U could be achieved by chemically extracting the protactinium during the reprocessing steps. The decay of this substance would result in uranium without the ^{232}U traces. However this is such a delicate process that the risk is relatively small. Thus, the proliferation risk of the thorium fuel cycle is substantially lower than that of the uranium fuel cycle [8].

TECHNOLOGICAL BARRIERS

Although thorium has a lot of advantages over uranium, uranium is by far the more dominant nuclear resource. Historically, this is due to the more excessive funding for uranium, because of its higher weaponization potential. In present times, thorium is still not utilized on a large scale, as technological problems limit its usage. Using uranium as nuclear fuel is more straightforward and less complex than utilizing thorium. There are a few barriers for using thorium. The fission of any uranium isotope generates about 2.4 neutrons. Hence, in a uranium fueled reactor it is allowed to "lose" 1.4 neutrons per fission. These neutrons are absorbed, scatter, or leak out of the reactor system. In the thorium cycle, the use of two neutrons per fission is needed, so the allowed "loss" in a breeder reactor is only 0.4 neutrons per fission. It is clear that this is a much smaller margin, and that thorium breeder reactors need a much more effective neutron economy. This includes materials with very low absorbtion to scattering ratios, and a low leakage geometry. Finally, there is a problem with the part of the decay scheme from ^{233}Th to ^{233}U. The decay to protactinium is very fast, however the decay of protactinium to uranium occurs with a half life of 27 days. In the meantime, a neutron capture reaction could induce transmutation of the protactinium into ^{234}U, which is non-fissionable. These effects combined make it difficult to raise the reactivity enough to reach criticality in a purely thorium fuelled system.

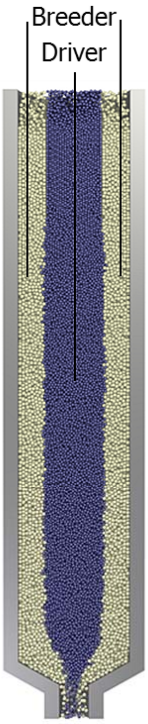

Figure 1.3: TB-HTR concept geometry

UTILIZATION IN HTRS

These problems are tackled partially by choosing an innovative reactor concept: the High Temperature Reactor. The structural material of this reactor core is almost exclusively graphite, which has a very low absorption to scattering ratio, making it a very effective moderator. Also, the coolant that is used, helium, is nearly invisible to neutrons, which is very favourable for the reactor neutron economy. Choosing the pebble bed type of this reactor allows flexible fuel management, as the pebbles are continuously removed at the bottom of the core, and can be added again at the top, hence "flowing" through the core in several passages. This means that a pebble with high protactinium content can be taken out of the reactor and given the chance to decay without parasitic neu-

tron capture. The reactivity of the system is further increased by choosing a specific design for the core. This design involves a central "driver" column, surrounded by a annular "breeder" column, as depicted in figure 1.3. The boundary between these zones might blur when the pebbles move axially through the core. However, studies have shown that this movement is negligible and the zone separation is well maintained within the predicted shape [9]. Fresh thorium-filled pebbles are added to the breeder column, and taken out of the system when enough thorium is transmuted in uranium and protactinium. These pebbles are reprocessed and their uranium content is put in new pebbles with high heavy metal loading. These pebbles have a high fissile uranium content, and are added at the top of the driver column. When the uranium content of the driver pebbles has decreased to a certain level, these pebbles are also reprocessed. The use of this geometry, with a driver channel and a breeder channel, is neutronically favourable as the reactivity in the core is enhanced due to the high uranium concentration in the driver. Also, the remaining neutrons escaping to the surrounding breeder channel allow for the transmutation of thorium. It has been shown that under this specific set of circumstances, equilibrium criticality can be reached by adding only thorium fuel. This means that the reactor has conversion ratio of 1, or in other words, it is a thorium reactor with net breeding.

1.4. RADIAL COOLING

COOLANT DIRECTIONS

Traditionally, high temperature reactors, including the pebble bed type, are axially cooled. As shown in figure 1.4, this means that the coolant flows vertically through the core, usually from the top to the bottom. This is realized by having a gas inlet that leads to a circular plenum, from where riser channels emerge. These riser channels are located all around the reactor core, and transport the coolant to a plenum at the top of the reactor. From here, the coolant flows through vertical slits in the top reflector, and into the pebble bed that comprises the actual reactor core. The coolant heats up while it flows through the power generating pebbles, and at the bottom it flows through a similar set of vertical slits in the bottom reflector. These lead to another plenum, from where the hot coolant flows through the outlet of the reactor core, and will be used to generate electricity. However, this is not the only direction in which coolant can flow through a High Temperature Reactor It is also possible to adopt radial cooling, which is visualized in figure 1.5. In this case, coolant flows radially through the core. This can either be from the inside to the outside, or from the outside to the inside. In both cases, a central "tube", positioned in the middle of the pebble bed, is required. Practically, this means that the pebble bed will take on a annular form instead of a cylindrical one, with a solid column inside. This column consists of a central vertical coolant flow pipe, surrounded with graphite in which there are horizontal slits to disperse coolant into the pebble bed. On the outside, there will be a similar layer of horizontal slits that will lead to vertical flow pipes distributed around the reactor core.

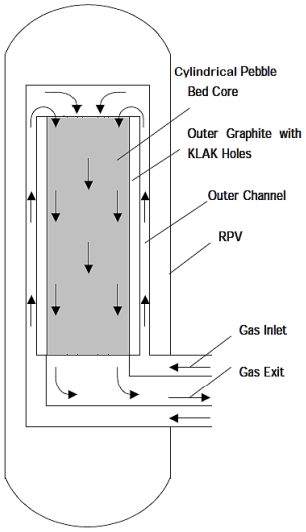

Figure 1.4: Axially cooled system

PROBLEMS INVOLVED IN AXIAL COOLING

This slightly more complex radial flow system is considered because there are a few disadvantages of the axially cooled system. First, the sleek design of the HTR, combined with the resistant inherent with flow through a packed bed, makes that forcing the coolant all the way from top to bottom of the core creates a relatively large pressure drop. For example in the PBMR design, this pressure drop can reach 2.8 bar[10]. The pumping power

required to move all the coolant through a system with such a pressure drop can be multiple percent of the net power output, hence this constitutes a quite substantial loss of efficiency. [11]. In thorium breeder HTRs this is even worse because adding the breeder zone calls for an increased mass flow, as the driver coolant will flow to the breeder zone if the same mass flow is not applied there.

Second, an inhomogeneous power distribution in the core causes problems. Since the flow through a pebble bed cannot be controlled so specifically, the temperature of the outflowing helium depends on the radius. In this case this means that the helium flowing through the center of the bed is a lot hotter than that in the outer side. In thorium breeder reactors this effect is stronger, as the driver channel has a much higher uranium concentration, and thus a much higher power density, than the surrounding breeder channel. This will cause high radial coolant temperature variations, and leakage of the hot helium from the driver into the breeder zone. The temperature variations will be undone as the coolant mixes in the outflow plenum, yet this effect decreases the thermal efficiency, and increases the maximum fuel temperature in the reactor. It is possible to drain the breeder outflow separately and use it to preheat the coolant. This partially resolves this problem, although it increases the system complexity and raises the pressure drop even further.

The third problem is one specific for thorium breeder pebble bed reactors. For all geometries, the neutron flux is lowest on the boundaries of the system. Hence, reactivity affecting components such as control rods and the emergency shutdown spheres will have less effect on the overall criticality of the system when placed in the side reflectors instead of at the center of the system. Although the German THTR-300 made use of control rods that penetrated into the pebble bed, this brought along quite a few complications. For example, the movement of the rods was relatively arduous due to pebble friction resistance, and a number of pebbles cracked due to the forceful penetration of the control rods. Fortunately for the pebble bed reactors, the reactivity effect of control rods in the side reflectors of a sleek reactor was strong enough to meet all safety standards. A thorium breeder reactor however already has a low neutron flux region in its breeder channel, and hence the flux in the reflector that surrounds it is extremely small. This means that reactivity measures placed there will have virtually no effect.

SOLUTIONS BY RADIALLY COOLING THE SYSTEM

The adoption of a radially cooled system could solve or at least strongly mitigate these problems. For one, the pressure drop trough the pebble bed is much lower for a radially cooled system than it is for an axially cooled one. This is because , an equal amount of coolant is pushed through a much wider effective area, for a much shorter distance. Theoretically, this can decrease the pressure drop by a factor of 100 [12]. Also, the outflow temperature variations will be greatly reduced due to the fact that all coolant is driven through both the driver as the breeder zone. This will also decrease the required mass flow. There will still be temperature variations due to the fact that the power density varies in the axial direction also. However these may be resolved by the fact that manipulation of the flow direction is much more potent. The central and side horizontal slits can be dimensionalized to induce specific mass flows at each core height. In axially cooled systems this is not possible because the effects will vanish long before a substantial part of the flow path is reached. In radially cooled systems this happens to a much smaller extent, again because of the wider flow area and shorter flow distance, and the fact that the coolant passes through both the driver as well as the breeder zone. Finally, inherently related to radial cooling is the use of a central reflector. It may be possible to use this reflector not only to guide the coolant flow, but also to place control rods in it.

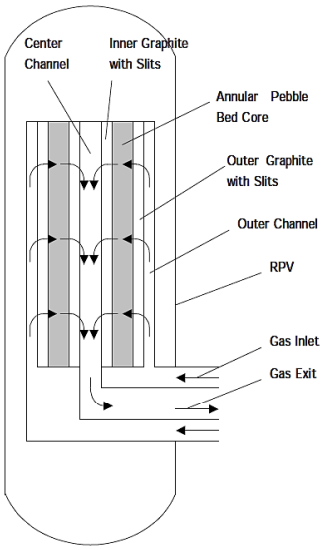

Figure 1.5: Radially cooled system

Since these will be in the center of the driver zone, the reactivity effect will be greater than when they would be placed in the side reflector [13]. The effects of the changed geometry on the conversion ratio cannot be easily predicted. On the one hand, it could be worse with a central reflector, simply because it occupies space and contains no fissile material. On the other hand it could improve, as the moderating power of the graphite in the central reflector will benefit reactivity.

1.5. AIM OF THE PROJECT

PROBLEM DEFINITION

The aim of the project is to investigate the potential benefits of radial cooling over axial cooling and propose a conceptual design for a radially cooled thorium breeder HTR. As a first estimation of the problems involved in axial cooling and the mitigation of these for a radially cooled system, MATLAB models are built for both an axially and a radially cooled system. These models will only consider thermal hydraulics. A homogenous power density will be assumed for both the driver and breeder channel, so no neutronic computations have to be included. It is expected that these models will be able to simulate the effects describing the pressure drop and the thermal helium mixing, that raises the outflow temperature related issues. The reactivity related problems can also be investigated without neutronics, since it is assumed that control rods in the central reflector will have enough reactivity worth to meet the safety standards. So the exact influence of the control rods on the criticality is not investigated, only the question if there is place for them in the central reflector.

STEADY STATE SIMULATIONS

These first investigations are not sufficient to reach sound conclusions. The adaptation of radial cooling may seem a solution to all the problems, but that would have to be verified by validated simulation codes. Also, unanticipated effects might come into play. In order to simulate all the relevant properties and visualize their effects, coupled neutronics / thermal hydraulics simulations are performed. They will be performed with THERMIX-DIREKT (a thermal hydraulic code specifically designed for pebble bed flow) and DALTON (a diffusion theory based neutronics solver). The output of one code is fed as input to the other, and vice versa. An iterative process is used to obtain a solution. In this way, both the temperature feedback on the neutronics, and the power density influence on the thermal hydraulics are taken into account. This will allow for a complete description of reactor behaviour in steady state operation. These calculations will be performed for both flow directions: outward as well as inward flow.

TRANSIENT SCENARIOS

The behaviour of the reactor in accident scenarios is of great importance as the safety of high temperature reactor technology is one of its key features. Therefore, transient scenarios are also simulated in this thesis. They are performed for two types of loss of cooling incidents. The first one is a Depressurized Loss Of Forced Cooling (DLOFC) incident, where the coolant circulation not only stops, but it also escapes the reactor until only atmospherically pressured helium is left. The second one is the pressurized variation (PLOFC). Here, the forced coolant circulation also stops, but the reactor remains pressurized, allowing better conductive heat transport via the helium and increased heat removal trough natural convection. It is assumed that a SCRAM occurs at the start of these scenarios, so that the fission reactions stop. Power is still produced by the decay of fission products in the core. These time dependent calculations will be performed for the thermal hydraulic effects only, using the way-wigner approximation to the decay heat production. LOFC scenarios without SCRAM are considered as outside the scope of this project.

THESIS OUTLINE

This thesis will continue with a description of the specific theory on the relevant thermal hydraulics, neutronics, and other physical concepts. It ends with a short description of the codes that are used. After this, the models that are used will be briefly introduced. Hereafter the results of the project will be shown. They will roughly follow the aforementioned pattern, starting with the preliminary MATLAB results, then go to the steady state coupled results, and continue to the transient scenarios. At the end of this chapter, effects of different flow directions are added. Finally there will be a conclusion, where the results will be discussed and recommendations will be made.

2

THEORY

2.1. THERMAL HYDRAULICS

In this section, the thermal hydraulic theory used in this research is described. First some general theory on flow through packed beds will be treated. The second part focusses on the pressure drop and finally there will be a section on heat transfer.

2.1.1. FLOW THROUGH PACKED BEDS

A pebble bed is a volume where spheres are randomly packed to form a granular medium. The packing fraction is defined as volume occupied by the particles divided by the total volume. For a pebble bed, this is equivalent to the number of pebbles times the pebble volume, divided by the total volume. This packing fraction can be used to define the porosity, or void fraction ϵ, as one minus the packing fraction:

$$\epsilon = 1 - \frac{V_{\text{spheres}}}{V_{\text{bed}}} \tag{2.1}$$

The value of this fraction depends on the ratio of the pebble diameter to the bed diameter. For this research, the value $\epsilon = 0.39$ is used, which corresponds to the average porosity found in the HTR-10 [14]. We define v_{p} as the mean velocity of the coolant between the pebbles. The velocity that describes the same flow through open volume, so without pebbles, is called the free velocity. The relation between these two quantities is given as:

$$v = \epsilon v_{\text{p}} \tag{2.2}$$

The hydraulic diameter for flow through a pebble bed is defined as four times the volume of the flow zone, divided by the area of the surrounding surface. [15]

$$d_{\text{h}} = \frac{4(v_{\text{total}} - v_{\text{spheres}})}{A_{\text{spheres}}} \tag{2.3}$$

Where the surrounding area, A_{spheres} is simply the total surface area of all the spheres, so N times the area of one sphere that can be expressed in terms of the volume and pebble diameter as:

$$A_{\text{sphere}} = \frac{6 v_{\text{sphere}}}{d_{\text{p}}} \tag{2.4}$$

Now, combining equations 2.1, 2.3 and 2.4, the hydraulic diameter of the pebble bed can be expressed in the pebble diameter and the void fraction:

$$d_{\text{h}} = \frac{2}{3} d_{\text{p}} \frac{\epsilon}{1-\epsilon} \tag{2.5}$$

The factor 2/3 arising in this relation is usually neglected [16],[15]. Using this hydraulic diameter and the mean velocity corresponding to the cross section of the bed derived in equation 2.2, we can define the Reynolds number for flow through the packed bed:

$$Re \equiv \frac{\rho v_p d_h}{\mu} = \left(\frac{1}{1-\epsilon}\right)\frac{\rho v d_\mathrm{p}}{\mu} \tag{2.6}$$

2.1.2. PRESSURE DROP

One of the key parameters of a reactor is the power required to pump the coolant through the core. A simple yet informative equation for the pumping power is given as : [16]

$$P_p \approx \dot{M}\frac{RT}{p}\Delta p \tag{2.7}$$

It can be seen from this equation that the pumping power is proportional to the mass flow and the pressure drop, and inversely proportional to the operating pressure. A certain mass flow is always required to remove the heat from the core, as can be seen in the following formula:

$$P_{\text{out, thermal}} = \dot{M} c_p \left(T_\text{out} - T_\text{in}\right) \tag{2.8}$$

The operating pressure p is limited because of economical reasons, especially with respect to the required containment strength. The pressure drop over the system can be influenced, and is of main importance to this research. The pressure drop resulting from forcing coolant to flow through a tube is described by the following relation:

$$\Delta p = f\frac{P_\mathrm{w} L}{A}\frac{\rho v^2}{2} \tag{2.9}$$

Where P_w is the wetted perimeter of the tube, L the length of the tube, A the cross sectional flow area, ρ the density of the coolant, v the coolant velocity, and f the friction factor that depends on the Reynolds number. Several correlations exists for the friction factor, the one that is used in this research is typical for helium flow: [16]

$$f = 0.01375\left[0.1 + \left(20\frac{\zeta}{d_\mathrm{h}} + \frac{10^3}{Re}\right)^{1/3}\right] \tag{2.10}$$

Here, the smoothness of the pipe surface is expressed by ζ, being the root mean square roughness. For this research this value is $45\cdot 10^6 m^{-1}$, a common value for pipes from industrial stainless steel. These equations can be used to determine the pressure drop for flow through cylindrical and annular tubes, and is used in this study to calculate the pressure drop trough all coolant flow pipes.

For coolant flow through a packed bed however, these equations do not hold, and more specific formulas are used. In case of flow through pebble beds, the pressure drop may be written as [15]:

$$\Delta p = \psi\frac{H}{d_\mathrm{h}}\frac{\rho v_\mathrm{p}^2}{2} \tag{2.11}$$

where H is the height of the bed, ρ the density of the coolant, $\mathrm{v_p}$ the coolant velocity, $\mathrm{d_h}$ the hydraulic diameter and ψ the pressure drop coefficient. Using equations 2.2 and 2.5, this transforms to

$$\Delta p = \psi\frac{H}{d_\mathrm{p}}\left(\frac{1-\epsilon}{\epsilon^3}\right)\frac{\rho v^2}{2} \tag{2.12}$$

Which is expressed in the free velocity and the pebble diameter. The pressure drop coefficient is a function of the Reynolds number. Several correlations can be found in the literature, the most common of them is valid for Reynolds numbers up to $5\cdot 10^4$ and is given by:

$$\psi = 320 Re^{-1} + 6 Re^{-0.1} \tag{2.13}$$

Wherein the two terms correspond to the asymptotic solution, the first for laminar flow and the second for turbulent flow.

2.1.3. HEAT CONDUCTIVITY

Due to axial and radial temperature gradients in the core, heat fluxes occur both parallel as normal to the main flow direction. The heat fluxes can be approximated using Fick's Law, which gives the heat flux as a function of the temperature gradients as follows:

$$\boldsymbol{q} = -\lambda \nabla T \tag{2.14}$$

For both directions, the effective conductivity λ can be expressed in a convective and a conductive plus radiative part in the following form [15]:

$$\lambda_{ax} = \frac{Pe}{K_{ax}}\lambda_g + \lambda_o \qquad \lambda_{ra} = \frac{Pe}{K_{ra}}\lambda_g + \lambda_o \tag{2.15}$$

Here the first term, describing the contribution of convection, uses the Péclet number Pe, the gas conductivity λ_g, and the parametric constant K, which is different for the radial and axial conductivity, and depends on the main coolant flow direction. For axial flow, K is given as:

$$K_{ra} = 8\left[2 - \left(1 - 2\frac{d_p}{D}\right)^2\right] \qquad K_{ax} = 1.3 \tag{2.16}$$

The second part of equation 2.15, λ_o, accounts for the radiative and conductive heat transport. It is defined as an addition of heat transport through the solid phase that consists of the graphite pebbles, and through the fluid phase of the helium between the pebbles. It is given as:

$$\lambda_o = (1 - \sqrt{1-\epsilon})\lambda_{gap} + \sqrt{1-\epsilon}\lambda_{fs} \tag{2.17}$$

The first term of this equation represents the heat conduction and radiation through the helium in the gap between neighbouring spheres. The second term corresponds to the heat conducted and radiated through the solid phase from layer to layer. The first term is given by:

$$\lambda_{gap} = \lambda_{gas} + \epsilon\lambda_{gas} Nu_r \tag{2.18}$$

Where λ_{gas} is the normal conductivity of the coolant gas. Nu_r is the radiative Nusselt number, that expresses the ratio of radiative to conductive heat transport in a medium. It is defined as:

$$Nu_r = \frac{4\sigma T^3 d_p}{(2/\epsilon_r - 1)\lambda_{gas}} \tag{2.19}$$

In this definition, σ stands for the Stefan-Boltzmann constant, and ϵ_r for the radiative emissivity, so not void fraction related.

The second part of equation 2.17, representing the heat transport through the spheres is given by the following formula, that is relatively complex due to the geometry of the random stack [15]

$$\lambda_{fs} = \frac{2\lambda_{gas}}{N-M}\left[\frac{BN-M}{(N-M)^2}\ln|N/M| - \frac{B-1}{N-M} + \frac{B+1}{2M}(N-M-1)\right] \tag{2.20}$$

Here, the factors M and N are functions of the ratio of gas and solid heat conductivity, defined as:

$$M = B\frac{\lambda_{gas}}{\lambda_{solid}} \qquad N = 1 + Nu_r\frac{\lambda_{gas}}{\lambda_{solid}} \tag{2.21}$$

Finally, B is a geometrical shape factor that depends on the packing of the bed as:

$$B = 1.25\left(\frac{1-\epsilon}{\epsilon}\right)^{1.1} \tag{2.22}$$

2.2. NEUTRONICS

2.2.1. NEUTRON DIFFUSION THEORY

The *Boltzmann neutron Transport Equation* is a balance equation for neutrons. It states that the time rate of change of the neutron concentration with a specific energy, time and place, equals the neutron production minus the losses. The neutron loss comprises two terms. The first one is any nuclear reaction that occurs, since this will always change the state of the neutron, that can be seen as loss of a neutron in that specific state. The second one is the leakage of neutrons from that specific spatial zone. The production is comprised of the neutrons released in fission events, and the neutrons that scatter from other energies and directions to the energy and direction considered. Reaction rates are actually determined by the neutron flux rather than the neutron density. This quantity equals the density times the velocity of the neutrons. The multi group transport equation is given as:

$$\frac{1}{v_g}\frac{\partial \phi_g}{\partial t} - \hat{\boldsymbol{\Omega}} \cdot \nabla \phi_g + \Sigma_{t,g}(\boldsymbol{r})\,\phi_g(\boldsymbol{r},t) = \sum_{g=1}^{G} \Sigma_{s,g\to g'}(\boldsymbol{r})\,\phi_g(\boldsymbol{r},t) + \chi_g \sum_{g=1}^{G} \nu_{g'}\Sigma_{f,g'}(\boldsymbol{r})\phi(\boldsymbol{r},t) \tag{2.23}$$

Here, the terms from left to right designate respectively: time rate of change of group flux, leakage, total reaction loss, inscattering, and the fission source term. The leakage term can only be defined in the neutron group current $\boldsymbol{J_g}$, where it is desirable to express it in the neutron group flux ϕ_g. It is impossible to express $\boldsymbol{J}$ in terms of ϕ in a general and exact manner. Hence, a approximation is needed. The approximation used in this research is an application of *Fick's law*, and is referred to as the *diffusion approximation*. In this approximation, the neutron current is assumed to be proportional to the gradient of the flux, with the diffusion coefficient as the proportionality constant. This yields:

$$\boldsymbol{J_g} = -D_g \nabla \phi_g \qquad\qquad D_g = \frac{l_{mfp,g}}{3} = \left[3\Sigma_{tr,g}\right]^{-1} = \left[3\left(\Sigma_{t,g} - \bar{\mu}_0 \Sigma_{s,g}\right)\right]^{-1} \tag{2.24}$$

Here the diffusion coefficient is defined as one third of the mean free path of the neutron. The inverse of the mean free path length is called the transport cross section, which is an artificial cross section that is defined using the total cross section, the scatter cross section, and the average scatter angle cosine. Implementing the diffusion approximation in equation 2.23 leads to the *multigroup diffusion equation*:

$$\frac{1}{v_g}\frac{\partial \phi_g}{\partial t} - \nabla \cdot D_g \nabla \phi_g + \Sigma_{t,g}\phi_g = \sum_{g=1}^{G} \Sigma_{s,g'g}\phi_{g'} + \chi_g \sum_{g=1}^{G} \nu_{g'}\Sigma_{f,g'}\phi_{g'} \tag{2.25}$$

The solution of this equation tends to be very close to the actual flux in media where the cross sections are weakly spatial dependent. For sharp transitions however, the diffusion approximation tends to make the result far less accurate. Hence, it is favourable to homogenize media, before performing diffusion calculations. For this research, only steady state diffusion calculations are performed. In this case, the time derivative is zero. For exactly critical systems, the equation would then hold. For other systems, the *multiplication factor k* is introduced. This factor adjust the magnitude of the fission source, so that the equation always has a solution. The situation where k equals 1 corresponds to a critical system, hence equal production and destruction of neutrons.

$$-\nabla \cdot D_g \nabla \phi_g + \Sigma_{t,g}\phi_g = \sum_{g=1}^{G} \Sigma_{s,g'g}\phi_{g'} + \frac{1}{k}\chi_g \sum_{g=1}^{G} \nu_{g'}\Sigma_{f,g'}\phi_{g'} \tag{2.26}$$

This equation can be solved by numerical methods, as will be treated further in section 2.4.2 of this chapter.

2.2.2. CROSS SECTION WEIGHTING

Calculations for the entire reactor could use the full cross section library that comprises the complete spatial dependent geometry and materials in the fine energy group structure. These calculations, however, are practically impossible due to the required computational time. Therefore, cross section libraries are prepared that preserve reaction rate, but use a coarser spatial and energy mesh. Cross section weighting is mainly used in two processes, energy group collapsing, and spatial homogenization. These will be treated in the following sections.

ENERGY GROUP COLLAPSING

Energy group collapsing is the process where a fine energy group structure is collapsed into a broad energy group structure. This means that the fine energy groups are combined in broader energy groups. For a very fine energy mesh, the flux has a predefined shape over the group interval. Such fine energy group cross sections can be treated as system invariant, and are collected in what are called master cross section libraries. Calculations of the full reactor core using this amount of energy groups are impossible in terms of calculation time. Hence, the cross sections need to be *collapsed* into broader energy groups. As mentioned before, this has to be done while maintaining reaction rates:

$$\Sigma_G \phi_G \equiv \Sigma_G \sum_{g \in G} \phi_g = \sum_{g \in G} \Sigma_g \phi_g \tag{2.27}$$

Where capital G stands for the broad energy group, and lowercase g for the fine meshed energy group. The broad group cross section can then be calculated according to:

$$\Sigma_G = \frac{\sum_{g \in G} \Sigma_g \phi_g}{\sum_{g \in G} \phi_g} \tag{2.28}$$

A weighting flux has to be found before the cross sections can be collapsed. This is frequently done by calculating the flux in a small part of the core, and use this flux to collapse the cross section in broader groups. Then the collapsed energy groups are used to perform calculations in the complex whole-reactor geometry.

SPATIAL HOMOGENIZATION

Homogenization of the cross sections is done in a similar way, by making sure that reaction rates stay equal over a specific cell. In this way, cross section variations due to spatial variations between zones z within the cell are accounted for effectively. The cell weighted cross sections are found by weighting the original cross sections with a weighting flux, while accounting for variations in the zone volumes V_z

$$\Sigma^j_{\text{cell}} = \frac{\sum_{z \in \text{cell}} [\Sigma^j_z \phi_z V_z]}{\sum_{z \in \text{cell}} [\phi_z V_z]} \tag{2.29}$$

Here also, the flux must be approximated before the cross sections can be homogenized over the unit cell. This is usually done by taking a small volume were a specific heterogeneity arises, and perform a full calculation over this volume. Then the homogenized cross sections can be used to perform calculations over larger volumes. This is especially useful in pebble bed HTRs, because of their double heterogeneity that arises from the coated microspheres and the pebbles itself. Homogenization is distinct from mixing in that it conserves reaction rates in the transition from a fine to a coarser spatial mesh, where mixing happens within a spatial mesh point.

The before mentioned cell-weighting is actually a specific variant of the more general cell-weighting where there is also group collapsing. These two can be performed simultaneously, using the follow-

ing formula:

$$\Sigma^{j}_{\text{cell,G}} = \frac{\sum_{g}^{G} \sum_{z \in \text{cell}} [\Sigma^{j}_{z,g} \phi_{z,g} V_z]}{\sum_{g}^{G} \sum_{z \in \text{cell}} [\phi_{z,g} V_z]} \tag{2.30}$$

Equation 2.30 is a simplification of this more general formula, with one fine group per broad group.

2.3. COUPLED CALCULATIONS

The interactions involved in coupled calculations can become extensive. Also, the type of time dependent problems performed and the decay heat treatment need to be explained. Therefore, it is necessary to introduce and elaborate several concepts. This is done in the following sections.

2.3.1. TEMPERATURE FEEDBACK

When the coupled behaviour of neutronics and thermal hydraulics of a nuclear reactor is modeled, two feedback mechanisms are of key importance. The neutronics determine where and how many fission reactions take place, hence providing the power density in the core. It should be clear that this is a key feedback mechanism on the thermal hydraulics part, as it determines the heat source term. The other feedback mechanism lies in the temperature distribution that is calculated in the thermal hydraulics part. The temperature has a strong influence on the neutronics, by a combination of multiple mechanisms.

First, cross sections are influenced by the Doppler effect. This effect arises when an atomic nucleus moves due to thermal vibrations. Because of this movement, the speed of an incoming neutron, and thus its energy, is changed in the nucleus reference frame. Hence, the vibrating nucleus "sees" the incoming neutron with a spread out energy. Resonances in the neutron absorption cross section are then widened, meaning that the neutron has a larger probability of being absorbed before it reaches thermal levels.

Another effect when the temperature rises, is that the thermal neutron energy will increase. This means that the flux spectrum shifts towards higher energies. This is enhanced in HTRs, by vibrations in the graphite lattice [17]. These vibrations increase when the temperature rises. They cause scattered neutrons to have an even higher energy. This leads to worse moderation inside the core, and higher energy of the neutrons scattered back into the core from the reflector. A consequence is that the leakage probability is higher, due to the enhanced speed of the neutrons.

Another consequence involves the thermal peak in the neutron spectrum. This peaks corresponds to the particles with the energy that corresponds to the temperature of the environment. For temperatures higher than the HTR operating temperature, this peak starts to overlap with the first resonance peak in the Uranium fission cross section. Hence the temperature has a positive feedback on the reactivity. However this effect is usually not strong enough to compensate all other effects, and the overall temperature feedback of a well-designed reactor will be negative. This means that the reactor is stable under power fluctuations. The shape of the power density is altered by the temperature in such a way that an increased local temperature leads to a reduced power density.

2.3.2. TRANSIENT SCENARIOS

When a reactor does not operate in steady state, its behaviour becomes time dependent, which is called a transient. Transient scenarios can vary from normal operating scenarios such as start up and controlled shut down of the reactor, to severe accidents. An important scenario is when the reactor experiences loss of forced cooling.

LOSS OF FORCED COOLING INCIDENTS

Loss of forced cooling means that the pumps stop working and forced convection ceases. This is a mayor incident in nuclear reactor operation, as forced convection is the most important way of heat removal from the core. It can happen in two distinct categories. The first one is Depressurized Loss of Forced Cooling (DLOFC). Under DLOFC conditions, the coolant escapes from the reactor core, until only atmospheric pressured helium is left. This coolant has such a low density that natural convection can be ignored and conduction and radiation are the only remaining heat transfer mechanisms. The second form is the Pressurized Loss of Forced Cooling (PLOFC). Here, the forced cooling also shuts down, but the primary circuit stays pressurized. This means that no coolant escapes from the core, and natural circulation adds heat removal capability to the heat transfer by conduction and radiation.

CRITICALITY CONTROL

Since in both these scenarios the main cooling method vanishes, emergency protocols dictate a complete shutdown of the reactor. This is done by full insertion of the control rods, hence reducing the reactivity so that the fission chain reaction is stopped immediately. This is what is called a SCRAM. There are excellent methods to ensure that the SCRAM takes place at all serious incidents, no matter what circumstances. However, this still is an active system, and it can fail. When a LOFC incident occurs, the temperature in the core will inevitably start to rise. This will stop the fission chain reaction because of the negative feedback on the reactivity. After this, strong neutron absorbing isotopes, such as ^{135}Xe, will accumulate in the core by decay of specific fission products. They will ensure sub-criticality of the reactor for at least a day. However, ^{135}Xe itself will then start to decay, and after some while xenon concentrations are sufficiently low and the temperature has dropped substantially, making the reactor critical again. This is referred to as re-criticality. So even for incidents where no SCRAM occurs, passive reactivity mechanisms will shutdown the reactor, although re-criticality can still be an issue. In this research, it has been assumed that a SCRAM takes place prior all transient.

2.3.3. DECAY HEAT

When an incident occurs in the reactor and subsequently a SCRAM is performed, the fission chain reaction stops. Although the power generated by fission is ceased completely, heat continues to be generated by the decay of fission products. In order to give precise predictions on the transient behaviour of reactors, this heat production must be determined accurately. The magnitude of this power depends on the number and type of radioactive isotopes present in the core at the time of shutdown. These follow from the equilibrium core nuclide concentrations. These concentrations are a complex function of the burnup, reactor type and operating time. Hence, calculating the decay heat can be a very time consuming job. Therefore a correlation for the decay heat fraction is used in this research. This correlation is the Way-Wigner approximation [18]. The assumption is that the power density after shut down is proportional to the nominal power density, and depends on the operating time of the reactor previous to the shutdown:

$$P(t) = 6.22 \cdot 10^{-2} \left[t^{-0.2} - (t + T_0)^{-0.2} \right] P_0 \tag{2.31}$$

Here $P(t)$ is the time dependent decay heat power, t the time after shutdown in seconds, T_0 the reactor operation time in seconds and P_0 the nominal operating power. In this research, this equation is averaged over the time step under consideration, and multiplied with the nominal power density in order to simulate decay heat production in that time step. The operating time before shutdown was assumed to be one year, which gives sufficient time for fission products to build up roughly to the equilibrium concentrations.

2.4. CODES USED

In this section, the theory behind the different codes used in this research is described. The first section will be a description of the thermal hydraulic pebble bed program THERMIX-DIREKT, which is shortened to THERMIX. Secondly, the neutronics diffusion solver DALTON will be treated. Finally, three SCALE modules, that where used for cross section preparation and temperature feedback implementation are discussed.

2.4.1. THERMIX

THERMIX-DIREKT is a combination of two codes, that are both specialized in pebble bed thermal hydraulics. THERMIX [19] is the radiative and conductive part, and DIREKT the convective part. In order to solve the thermodynamic equations, the code needs the nuclear power density, geometry, and an initial guess for the temperature distribution. It can operate both in time dependent, and steady state mode. A steady state calculation starts with performing THERMIX under the assumption that there is no convective heat transport. The acquired results are used by DIREKT to compute the coolant flow, and the resulting convective heat source is fed back to THERMIX. This process is repeated iteratively until the convergence criteria are reached. A time dependent calculation always needs a restart file. For the first time step, this contains the relevant properties from a steady state calculation. Now THERMIX and DIREKT are run subsequently, and their results are stored in a restart file with updated time stamp. Both of these two modules will be treated in detail in the next sections.

CONDUCTIVE

THERMIX uses the power density to calculate the thermal hydraulic properties arising from conductive and radiative transport. The treatment of heat transfer in traditional geometries such as pipes and plena is similar to common CFD codes, and will not be discussed here. For the pebble bed, a specific type of heat transport is computed. This heat transport is due to heat conduction through the pebble and the coolant gas between the spheres plus the superimposed thermal radiation exchange between sphere surfaces. This is described by the Fourier equation with temperature dependent material constants [20]:

$$\rho_s(T)C_s(T)\frac{\partial T}{\partial t} = \nabla\cdot(\lambda_0(T)\nabla T) + q_n''' + q_c''' \tag{2.32}$$

Here, ρ_s and C_s are the density and heat capacity of the solid, T is the temperature of the solid, λ_0 is the effective conductivity earlier defined in section 2.1.3, and the two volumetric heat sources, are q_n''', the nuclear power density and q_c''', the convective contribution. The initial guess for the first iteration is that there is no convection, hence q_c'''=0

This equation can be multiplied with the volume element, and a cylindrical geometry can be adopted, which leads to the following numerically solvable equation:

$$\rho_{\text{solid}}C_{\text{solid}}\frac{\partial T}{\partial t}dV = d\left(\lambda_0\frac{\partial T}{\partial \ln|r|}\right)2\pi dz + d\left(\lambda_0\frac{\partial T}{\partial z}\right)2\pi r dr \tag{2.33}$$

It must be noted that per spatial interval, only one temperature occurs in this equation. This does not account for differences in the pebble. When the heat production is significant compared to the speed of heat removal, this assumption is not valid. Exact fuel temperatures are needed for the neutronics part, and to determine the maximum TRISO temperature. Hence, the heterogeneous solids temperature option has to be used for steady state calculations. For transients with SCRAM, low decay heat production and good thermal heat conductivity cause negligible difference when hetero/homogeneous temperature treatment is applied, as is shown later in this research.

CONVECTIVE

DIREKT, the convective module, starts with calculating the coolant flow. This involves solving the momentum equation and the equation of continuity, which gives the mass flow vectors and Reynolds numbers. Then, the gas temperature is computed, by solving the equation of state and the energy equation. This calculation results in the gas temperatures and the heat transfer coefficients [21]. Combining these with the solid temperature calculated in the conductive part, the convective heat source is made explicit using Newton's law of cooling:

$$q_c''' = \alpha A \left(T_{\text{solid}} - T_{\text{gas}} \right) \tag{2.34}$$

Where the volumetric heat source equals the heat transfer coefficient times the contact area times the temperature difference. The convective heat source is fed back to THERMIX, that updates its properties. This circle goes round iteratively, until the convergence criteria are reached.

2.4.2. DALTON

DALTON is a diffusion theory based neutronics solver, that can run in both time dependent and steady state mode. In this research, DALTON is used only in steady state mode. In this mode, it solves the *steady state multi group diffusion equation*, as given in equation 2.26. This is achieved by applying the power method. The exact principles of the power method are excessively treated in several mathematical textbooks [22] and only the general idea will be provided here. We can express the group fluxes in a vector and rewrite the steady state multi group diffusion equation as a matrix vector equation. This leads to the following generalized eigenvalue problem:

$$\boldsymbol{M}\vec{\phi} = \frac{1}{k}\boldsymbol{F}\vec{\phi} \Longleftrightarrow \boldsymbol{M}^{-1}\boldsymbol{F}\vec{\phi} = k\vec{\phi} \tag{2.35}$$

Where the destruction operator M is defined as:

$$\boldsymbol{M} = -\nabla D \nabla + \Sigma_t - \sum_{g=1}^{G} \Sigma_{s,g'g} \tag{2.36}$$

And the production operator F as:

$$\boldsymbol{F} = \chi_g \nu_{g'} \Sigma_f \tag{2.37}$$

Hence the only neutron production mechanism is by fission. The eigenvalue problem given in equation 2.35 has multiple eigenfunctions, or modes, with associated eigenvalues that can be ordered in size:

$$|k_1| \geq |k_2| \geq |k_3| \geq \cdots \geq |k_n| \tag{2.38}$$

The dominant eigenvalue, k_1 equals the effective multiplication factor k_{eff}. The principle of the power method is the subsequent multiplication of an arbitrary initial flux $\vec{\phi}_0$ with the matrix $\boldsymbol{M}^{-1}\boldsymbol{F}$, such that:

$$\vec{\phi}_{l+1} = \left[\boldsymbol{M}^{-1}\boldsymbol{F}\right]\vec{\phi}_l = \left[\boldsymbol{M}^{-1}\boldsymbol{F}\right]^2\vec{\phi}_{l-1} = \cdots = \left[\boldsymbol{M}^{-1}\boldsymbol{F}\right]^{l+1}\vec{\phi}_0 \tag{2.39}$$

Now the ratio of the subsequent vectors $\vec{\phi}_{l+1}$ and $\vec{\phi}_l$ will tend to the effective multiplication factor, and $\vec{\phi}_{l+1}$ to its associated eigenvalue or mode, which is the neutron flux in the reactor.

$$\lim_{l\to\infty} \vec{\phi}_{l+1} = \vec{\phi} \qquad \lim_{l\to\infty} \frac{\vec{\phi}_{l+1}}{\vec{\phi}_l} = k_{\text{eff}} \tag{2.40}$$

This flux is an eigenfunction, and hence it can be scaled with an arbitrary value while remaining a solution to the eigenvalue problem. This flux can be used to find the fission density, and hence the power density, by multiplying it with the macroscopic fission cross section map. Because the power density follows from the neutron flux, it actually defines a power density distribution, that can be raised or lowered to achieve the desired total reactor power.

2.4.3. SCALE

SCALE, or Standardized Computer Analyses Licensing Evaluation, is a modular code system developed by Oakridge National Laboratory at the request of the US Nuclear Regulatory Commission. Its purpose is aimed at problem dependent cross section generation, analysis of criticality safety, shielding, heat transfer and depletion/decay schemes. Three of its modules were excessively used in the preparation of the cross sections, and will be treated henceforth.

CSASI

The Critical Safety Analysis Sequence is a module of SCALE that provides for automated, problem dependent, cross section processing followed by calculation of the neutron multiplication factor for the system being modeled [23]. The nuclide content of the reactor is known, and hence it is favourable to define the macroscopic cross sections for each spatial position. In order to achieve this, CSASI calls several other SCALE modules, such as XSDRNPM and ICE. CSASI performs cell weighting and mixing using the following definition.

$$\Sigma^j_{cell,E} = \sum_{z\in\text{cell}} \left[f_{z,E} N^j_z \sigma^j_{z,E} \right] \tag{2.41}$$

Here, the microscopic cross section $\sigma^j_{z,E}$ is multiplied with the concentration of nuclide i in zone z, leading to the macroscopic cross section. The weighting is done with the flux disadvantage factor, which follows from XSDRNPM as:

$$f_{z,E} = \frac{\phi_{z,E} \sum\limits_{z\in\text{cell}} [V_z]}{\sum\limits_{z\in\text{cell}} [\phi_{z,E} V_z]} \tag{2.42}$$

This factor accounts for differences in the neutron flux and zone volume, to conserve reaction rates in the homogenized cell.

XSDRNPM

XSDRNPM is a 1D transport solver which computes the neutron flux for spherical, slab or cylindrical geometries using a criticality calculation [24]. It is able to collapse energy groups weighted with this flux, while maintaining reaction rates in designated spatial zones z:

$$\Sigma_{G,z} = \frac{\sum_{g=1}^{G} \Sigma_{g,z} \phi_{g,z}}{\sum_{g=1}^{G} \phi_{g,z}} \tag{2.43}$$

It hence produces a set of broad group cross sections for that specific zone. XSDRNPM can also perform cell weighting to reduce spatial discretization besides energy group collapsing.

ICE

ICE, or Intermix Cross sections Effortlessly [25] can homogenize areas and mix cross section contributions from various origins, using:

$$\Sigma_{\text{eff}} = \sum_i f_i \Sigma_i \tag{2.44}$$

Where the sum of the factors f_i equals one. This can for instance be used to mix nuclides, where the factors are the relative nuclide densities. It can also be used to mix the cross sections derived for different conditions. For example, cross sections can be determined for two distinct temperatures. When a cross section is required for a temperature between these two, it can be defined by interpolation between the two predetermined cross sections. The cross section mixing then takes on the form:

$$\Sigma_T = f_{T_a}\Sigma_{T_a} + f_{T_b}\Sigma_{T_b} \qquad f_{T_a} = \frac{T_b - T}{T_b - T_a} \qquad f_{T_b} = \frac{T - T_a}{T_b - T_a} \tag{2.45}$$

The interpolation coefficients have to be determined externally, and then ICE can mix the cross sections. This way of cross section mixing can be used to account for temperature feedback. The exact method that is used in this research is treated in section 3.3

3

MODELS

Several models were used in this research, and will be described in this chapter. First, two pebble bed reactor models were built in MATLAB. In these semi-analytic MATLAB models a combination of analytic relations and numerical computations were utilized. One of these modelled an axially cooled reactor to visualize the effects of hot and cold helium mixing. The other model represents a radially cooled reactor, and was build to investigate the feasibility of forcing the coolant through the core in such a way that sufficient cooling reaches each location in the entire core.

After these preliminary computations, the radially cooled core was modeled to further extend with THERMIX, which is a specific pebble bed thermal hydraulics code. Furthermore, cross sections where prepared for the radially cooled geometry, and these were used to model the neutronics of the reactor with DALTON. These two models were then used in an iterative scheme to perform coupled thermal hydraulics / neutronics calculations, in order to achieve a complete description of the steady state reactor behaviour. The steady state circumstances were used as a basis for time dependent transient calculations, as will be treated in section 3.3.2.

3.1. SEMI ANALYTIC MATLAB MODELS

Two reactors were modeled in MATLAB, one with axial cooling and one with radial cooling. The geometry of these models is visualized in figure 3.1. The power density was assumed to be constant at $3.2 MW/m^3$ over the entire driver volume, which corresponds to the average power density in the HTR-PM. Over the entire breeder zone, the power density was assumed constant at $0.3 MW/m^3$. In the axially cooled core, the driver and breeder radii were taken as 1.5 and 2.5 meter respectively, leading to a total thermal power of 290 MW. In the radially cooled core model, a 50 centimeter radius central reflector is added, through which the coolant flows into the core. In order to make representative comparisons with the axially cooled core, the driver and breeder radii were adjusted to 1.58 and 2.55 meter respectively, to conserve the channel volumes, and hence the total power. Both these models will be treated in further detail in the next sections.

3.1.1. AXIAL COOLING

In the axially cooled model, the uppermost region is the source of a purely vertical mass flow. This simulates the vertical inflow through the upper slits. The coolant then travels through two adjacent zones, the driver and breeder channel, as is visualized in figure 3.1. These channels have different power densities, which leads to variations in temperature, and hence density, for the two channels. This results in a small amount of radial mass flow from the driver into the breeder channel. The outflow was modeled with purely vertical mass flow, again to model for the slits. When the driver

coolant expands faster than the breeder coolant density, some driver coolant will start to invade into the breeder zone. In the first version of the model, diffusive heat transport at the breeder/driver channel interface was neglected. In this way, the only heat transport over the boundary is convective heat transport, as the driver coolant is hotter than the breeder coolant. The border between these flows was modeled as an absolute thermal boundary. In this way, the magnitude of the hot helium leakage stream was determined. In the second version, heat diffusivity across the boundary was also taken into account, to model a more realistic reactor. This involved application of the heat transport theory described in section 2.1.3.

3.1.2. RADIAL COOLING

In the radially cooled core model, the top and bottom slits present in the axially cooled model were replaced with smooth boundaries. It further involved the placement of a central vertical coolant flow zone, surrounded by a reflector, wherein the horizontal slits are located. Finally, the exterior slits and corresponding vertical flow plenum where added to the side of the reactor. The coolant inflow is located at the bottom center. When it flows up through the central pipe, the pressure drops according to equation 2.9. As the core has a homogeneous power density, homogenous outflow temperatures are reached when the radial mass flow into the core does not vary with height. This leads to a constraint on the z-dependent slit pressure drop, from where the required slit parameters are derived. This has been achieved by rewriting equation 2.9 as a function of flow area. Hence, the presumed pressure drop leads to the fraction of the central reflector cross sectional area that has to be reserved for coolant flow paths. This in contrary to normal practice, where the pressure drop follows from the given parameters. As the flow paths are slits through graphite, the root mean square roughness was raised to 1 mm. When the coolant flows through the core its density decreases due to thermal expansion, and the pressure drops further. Then the coolant flows through the outer slits, down again through the exterior vertical pipes, and out of the system at the bottom outside of the core. The exterior slit parameters are again calculated in such a way that radial mass flow variations are reduced.

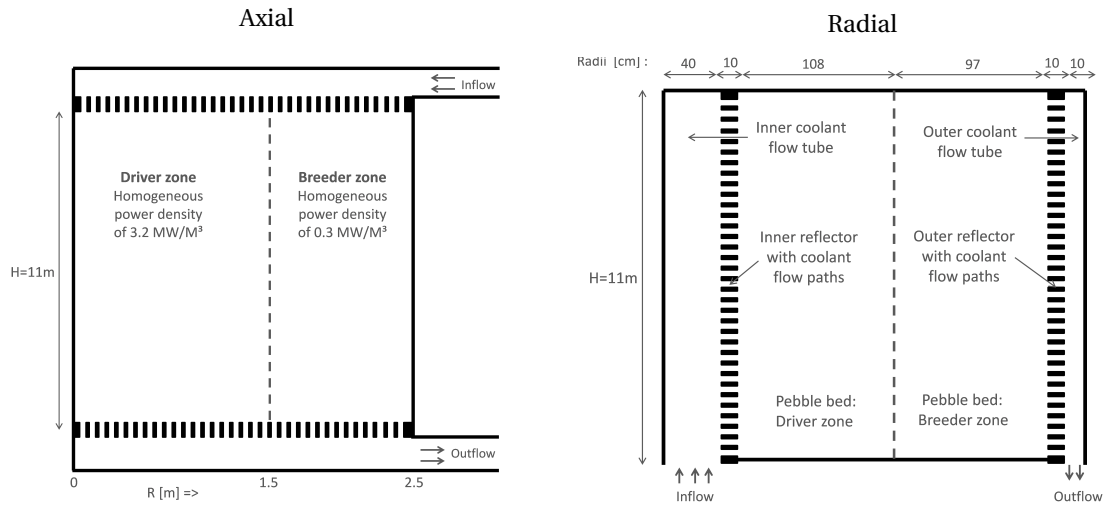

Figure 3.1: MATLAB models of pebble bed reactor cores with different coolant flow directions. For both the breeder and the driver zone, volumes and power densities are equal in both models

3.2. THERMAL HYDRAULIC THERMIX MODEL

In THERMIX [26], the radially cooled core was modeled in a more detailed geometry, that will be described below. THERMIX is a 2D program, where a parametrization is used to simulate the effects of azimuthal variations in geometry, materials and flow. For every region, a specific flow type must be defined. This can be: exclusively horizontal flow, exclusively vertical flow, flow in both directions or no flow at all. Each of these zones has a solid and a fluid fraction, determined by the porosity ϵ. Coolant flow pipes can be simulated by defining a hydraulic diameter with its corresponding porosity [27]. The fluid type has to be specified, in this research it is helium gas. The solid is specified for every specific region, and consists mainly of different types of graphite. A difference with the MATLAB geometry is that the coolant inflow is not located at the center of the reactor, which is undesirable as in this case the fresh helium cannot be used to cool the side of the reactor. Instead, the coolant inflow is located at the outside of the core at one meter above ground, into an annular plenum. From this plenum, the coolant flows in upward direction at the side of the reactor, through vertical flow channels called risers. These risers transport the coolant to another annular plenum, from where the coolant flows to the top center of the reactor, and into the central vertical coolant flow pipe. The coolant then flows through the horizontal slits into the pebble bed, and out through another set of slits that lead to vertical pipes surrounding the bed. Then, the coolant flows to the bottom of the reactor, where it is collected in an annular ring. From here the coolant flows out of the part of the reactor that is modeled. The thermal boundaries surrounding this flow system are modeled to represent the conditions of the HTR-PM [3]. There are strong thermal isolation layers at the top and bottom of the reactor. It is assumed that the heat transfer through the top and bottom of the core is negligible. This is desirable as the radial exterior comprises a water cooled panel, which is assumed to have a much higher heat removal capacity than the top and bottom boundaries. A variation from the HTR-PM design is the removal of the second helium gap and metallic internals at the top and bottom of the reactor. The heat flow in these directions is not significant due to the strong insulators, hence this is a reasonable simplification.

3.2.1. CONDUCTIVE MODEL GEOMETRY

As is shown in figure 3.2, the center of the model consists of an 11 meter high, 40 centimeter radius vertical coolant flow zone. This zone is surrounded by a 10 centimeter porous graphite horizontal flow zone, to simulate the pipe wall with coolant flow slits. These two zones together form the central reflector. Surrounding the reflector is the annular pebble bed zone. This zone is the most important one, and hence it is relatively fine meshed with 44 axial and 22 radial intervals. After this zone there is again a 10 centimeter wide horizontal flow area to simulate the outer coolant flow slits. These slits lead to vertical flow pipes, where a porosity of 0.58 simulates the placement of 24 open flow pipes. The space between the pipes is filled with reflector graphite. This type of graphite is also present in the surrounding region, which is a 14 centimeter wide no flow area. Around the reflector the riser channels are embedded, again in reflector graphite, with a porosity of 0.2. The total core is surrounded by a different type of graphite, carbon brick, that acts as thermal reflector. The outside of the reactor consists of a helium gap region, a metallic internals region, another helium gap and then the Reactor Pressure Vessel (RPV). At the top and bottom of the reactor, the reactor pressure vessel was modeled with an almost negligible thermal conductance, creating a thermal insulator. This led to the omission of the axial metallic internals and second helium gap in this model, as they are redundant heat boundaries.

The insulators force almost all heat to be transported radially out of the system. This is done because the radial boundary is a water cooled panel, which has a very large heat removal capability. The water cooled panel was modeled to be subject to sufficient cooling to keep the temperature at 70 °C. The PRV is surrounded by air, and placed in a dome, which is modeled as a layer of concrete. This layer was used as top and bottom boundary of the model. The heat transfer in these directions is

relatively small, hence it was assumed that this region maintained a 20 °C temperature. In the radial direction, the boundary condition was already defined for the water cooled panel, and the concrete dome was not included in the model. For a complete THERMIX description of the materials and position of each zone, the reader is referred to appendix B.

3.2.2. CONVECTIVE REPRESENTATION

It must be noted that for the convective part of the code, only the flow areas are needed. Hence, in this part only regions 1 till 20 are defined, and the remaining components are described as a no flow area. The inner vertical coolant flow pipe is modeled as a completely open coolant flow zone ($\epsilon = 1$). The other vertical zone areas consist of multiple pipes. For these pipes, a specific parametrization for the hydraulic diameter and porosity is used. For the vertical outflow region, this corresponds to 24 evenly placed pipes with a diameter of 40 centimeter. For the risers, they simulate 20 pipes with a diameter of 20 centimeter. The plena and horizontal flow tubes are modeled as high porosity, two dimensional flow zones. The pebble bed is modeled with the parameters according to the stacked bed thermal hydraulics described in section 2.1.1. In order to achieve a specific mass flow through all parts of the pebble zone, both horizontal slit zones were divided in 22 subzones in the convective model. This allows for variation of the slit hydraulic diameter with height. In order to reach a more homogenized outflow temperature, the slit diameters are determined from the axial differences in coolant temperature. This proceeds in an iterative method until a specific criterium for the temperature variations is reached.

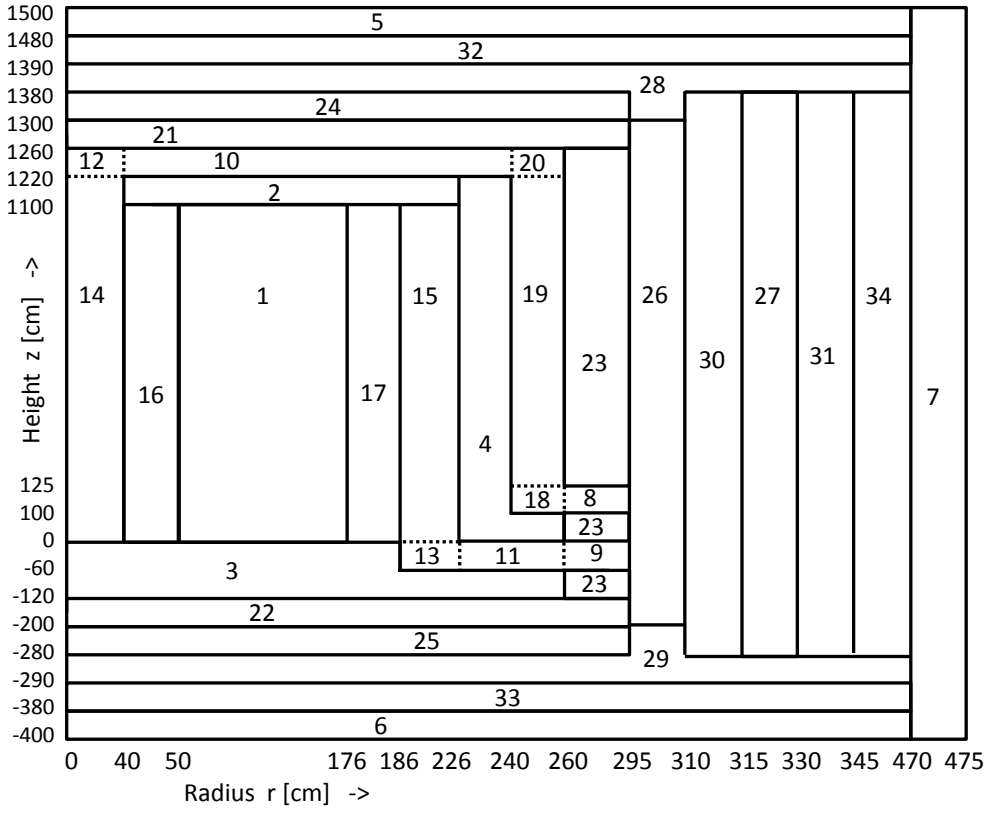

Figure 3.2: THERMIX conductive model, with components; 1: Pebble bed, 2-4: reflector, 5-6: concrete boundary, 7:water cooled panel, 8 inlet, 9 outlet, 10-11 horizontal flow zone, 14,15,19: vertical flow zone, 16,17 horizontal slits. 12,13,18,20: plenum, 21-23: carbon brick, 24-27: helium gap, 28,29: insulator, 30: metallic internals, 31 RPV, 32:34 air gap.

3.3. COUPLED SYSTEM MODEL

In fully coupled mode, THERMIX interacts with DALTON according to figure 3.3. The coupling of DALTON to THERMIX is a well known and validated procedure [28], [29]. In the coupling scheme, collapsed temperature dependent cross section data for every location in the reactor core is needed. These cross section libraries are created for specific sets of constant fuel and moderator temperatures, where the reflector temperature equals the moderator temperature. There are 25 of these temperature combinations, which arise from any combination of 300, 700, 1100, 1500 and 1900 Kelvin for the fuel and moderator temperature. The details on how these collapsed cross section libraries are prepared are given in the next section. ICE mixes the cross sections from the temperature dependent libraries into a single library. This is done for every core location by interpolation between the libraries with temperatures closest to the temperatures at that location. The combination of fuel cross sections is done by a double linear interpolation between the libraries with nearest fuel and moderator temperatures. The moderator cross sections dependence on the fuel temperature is not significant, hence only a single linear interpolation between the libraries with closest moderator temperature and 1100 Kelvin fuel temperature is used. The temperature corrected cross section map is used by DALTON to solve the multi group diffusion equation, to find the neutron flux and power density [26]. The model in DALTON is equal to the THERMIX model for the zones 1-20. At the outside of this region, the reactor is modeled with reflector material and a vacuum at the boundary. This is done because with the combined reflector graphite from the porous slits, reflectors, and coolant pipes, the effective reflector thickness is more than 59 centimeter, which is the thermal neutron diffusion length in graphite [30]. As the neutron flux in the breeder zone is already reasonably low, the material differences outside the reflector are assumed to have no significant influence on the core flux. The power density is then used as source term in THERMIX. THERMIX calculates the thermal hydraulic properties of the coolant and solid part of the core, and gives the updated temperature profile for interpolation by ICE. This process is repeated in an iterative manner until convergence is reached.

It must be noted that this convergence is reached far more quickly due to the inner slit determination iteration. This iteration aims to homogenize the outflow temperatures, which reduces the dependence of the temperature profile on the power density. This makes that the THERMIX/DALTON iteration converges in just a few steps, which is fortunate since it is the most time consuming part.

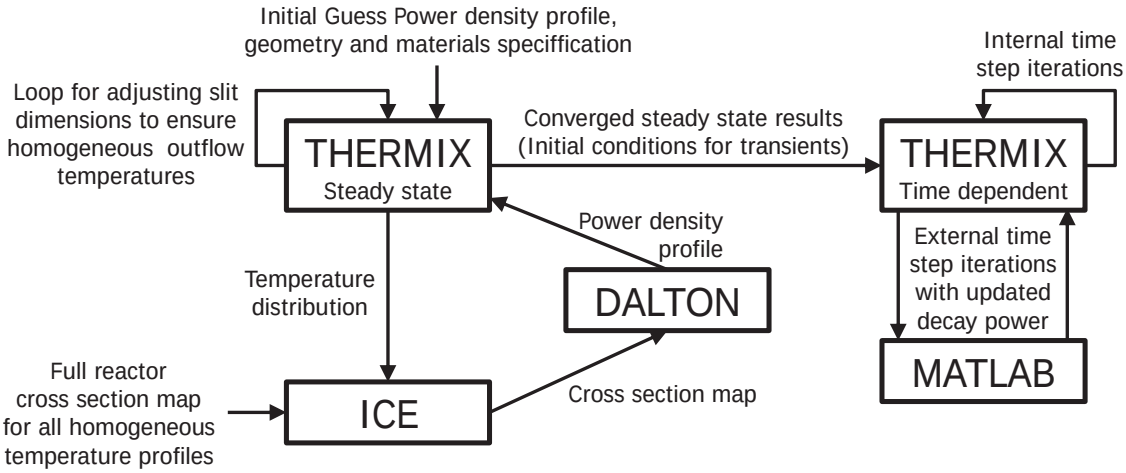

Figure 3.3: Scheme of the codes used in the coupled model. The main loop for steady state calculations is the DALTON/THERMIX/ICE triangle.

3.3.1. CROSS SECTION PREPARATION

The cross sections of the pebbles can only be calculated when the nuclide concentrations within the micro spheres is known. In this research, the concentrations are taken from the equilibrium condition of an axially cooled thorium breeder pebble bed reactor [31]. For each temperature profile, the corresponding cross sections are homogenized in three steps. First, they are weighted over the fuel kernel plus coating layers. Then they are weighted over the micro spheres embedded in graphite in the fuel zone of the pebble. Finally they are weighted over the full pebble plus a layer of surrounding coolant. This results in an homogenized cross section library for the pebble bed. These cross sections are, location specific, collapsed in five energy groups using two XSDRN calculations. The energy group boundaries are depicted in table 3.1. In these calculations, the packing fraction is assumed constant over the entire core. This is not the case in reality, as in close proximity of the walls, the packing fraction tends to oscillate around the average value [32]. However, the effects of the difference in pebble fraction on the criticality calculations are small. One of the XSDRN calculations is in the radial direction, and is used to collapse the cross sections of the central reflector, pebble bed and radial reflector zones. The other one is an axial slab calculation, which uses bucklings factor to account for the finite radius. This one is used to collapse the top and bottom reflector zones. As already mentioned this process is performed for the 25 temperature combinations of moderator and fuel temperature. The libraries are then ready to be used by ICE.

Table 3.1: Group boundaries for the energy structure used in DALTON

Group number	Upper boundary (eV)	Lower boundary (eV)
1	2.00E+07	9.00E+05
2	9.00E+05	3.00E+01
3	3.00E+01	6.25E-01
4	6.25E-01	1.50E-01
5	1.50E-01	1.00E-05

3.3.2. TIME DEPENDENT CALCULATIONS

The transients, as treated in section 2.3.2, start from steady state conditions. Hence, the results from a steady state calculation are used as an initial condition for this simulation. At t=0, a SCRAM occurs, causing the power profile to drop to the value predicted by the Way-Wigner approximation treated in section 2.3.3. In the case of a DLOFC incident, the system depressurizes instantaneously. The time discretization has two steps, an outer step with updated decay heat profile, and an inner step in THERMIX. The scheme of this time discretization is different for the DLOFC case than for the PLOFC case, as in the latter, the natural convection plays an important role. For the DLOFC case, the first 10 time steps equal 10 seconds for the outer iterations, and 0.1 for the inner ones. Then, 9 steps are used of 100 and 1 second respectively. After this, the remainder of the transient is calculated with outer steps of 1000 seconds and inner steps of 10 seconds. These step sizes are not sufficient for correct calculation of the natural convection, hence a finer time mesh is needed for the PLOFC calculation. The same scheme as before is used, but the values are divided by 10.

4

RESULTS

4.1. SEMI ANALYTIC MATLAB MODEL

Two models were built in MATLAB. A detailed specification of these models is given in section 3.1. The first model represents an axially cooled core and was used to quantify the effects related to radial variations in coolant temperature. The second model was used to investigate the feasibility of pumping coolant radially through the core. Special focus lies on the central reflector dimensions needed to ensure sufficient coolant flow in the entire core, while reserving enough space for the control rod system. The results of these computations will be treated in further detail in the next two sections.

4.1.1. AXIALLY COOLED

For the axially cooled core, only convective heat transport was included in the first version of the model. This means there was no thermal diffusivity between the coolant flow through the breeder zone and through the driver zone. The only heat transfer between these zones was due to the faster expansion of the coolant in the driver zone, causing this hot coolant to enter the breeder zone. This was modeled by the creation of a third flow area, in which ideal thermal mixing was assumed. At every core height, the axial pressure drop was kept constant over the radius. This leads to an amount of hot driver helium entering the third flow area, which caused the volume and averaged temperature to increase while traversing the height of the reactor core. The temperature profile

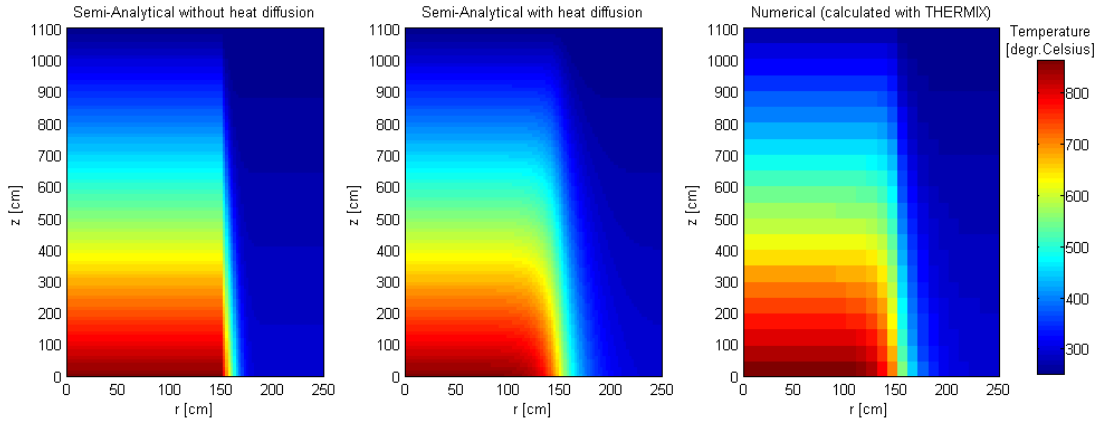

Figure 4.1: Helium temperature profile for the MATLAB models with and without thermal diffusivity, and the temperature profile computed with THERMIX to serve as benchmark.

resulting from this first version of the model with axial cooling is visualized in the left graph of figure 4.1.

This version takes into account only the intrusion of the driver coolant in the breeder zone, but the effect of heat transport at the driver/breeder flow interface will have a major influence on the results, especially with the large temperature differences at this interface. Hence, this version of the model was considered not accurate enough to make a realistic quantification of the radial outflow temperature variation and the associated thermal efficiency loss.

Therefore a second version of the model was created, in which the heat transport theory presented in section 2.1.3 was used to add the effects of thermal diffusivity. The results of this can be seen in the centre graph of figure 4.1. To validate the code, the temperature was compared to a numerical THERMIX simulation with similar parameters, shown in the right graph of figure 4.1. It can be seen that the results of the second version of the model were in far better agreement with this reference case than the results of the first version of the model. This second model, with heat diffusivity, was used to quantify the factors influencing the thermal efficiency.

To maximize the thermal efficiency, the temperature difference between inlet and outlet must be maximized. Hence, it would be best to use only the hot driver coolant, without mixing it with the relatively cold coolant flowing through the breeder zone. Yet part of the thermal energy would be lost, which is unacceptable as it will strongly decrease the total efficiency of the system. The effects of separately removing the hot helium flow depends on the radial position of the stream separation. In figure 4.2, the temperature of the hot coolant channel outflow and the thermal power it contains are plotted as a function of the radial position of the stream separation.

Clearly, it is not possible to combine high outflow temperatures with minimal energy losses. This means that a substantial part of the flow cannot be used directly for efficient conversion to electrical energy. This fraction has to be pumped through the reactor once more. This way, the energy would be used to preheat the coolant and in principle no efficiency would be lost. However, the pressure drop of forcing the breeder coolant up and down through the entire core again would almost double the already large pressure drop for the once through flow scheme. This would have a large effect on the efficiency of the system, as the required pumping power would increase. Hence, it is clear that the pressure drop over an axially cooled system is significant, especially for a thorium fueled system with a low power generating breeder zone.

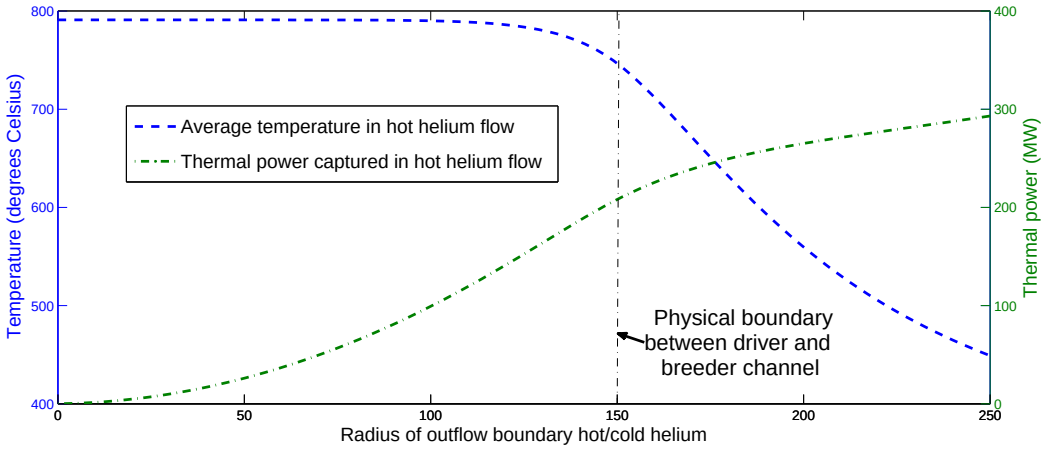

Figure 4.2: The effects of the stream separation location on the parameters of the hot part of the coolant. If the boundary is placed to the left of the physical zone boundary, the temperature is maximal but a large part of the energy is lost. To the right of the physical boundary, most of the energy is utilized, but the average temperature decreases significantly.

4.1.2. RADIALLY COOLED

For the radially cooled core, attention was focussed on the pressure field. The pressure drop for the components of the model depicted in figure 3.1 were calculated according to the equations given in 2.1.2. Since this model assumes uniform power density, the desired mass flow was constant over height. In this case the pressure drop resulting from radial flow through the bed is also constant over height. This means that for this model, the slit dimensions have to be defined in such a way that their axial variation exactly cancels the pressure drop over the vertical flow pipes in the inner and outer reflector. This leads to the pressure profile depicted in figure 4.3.

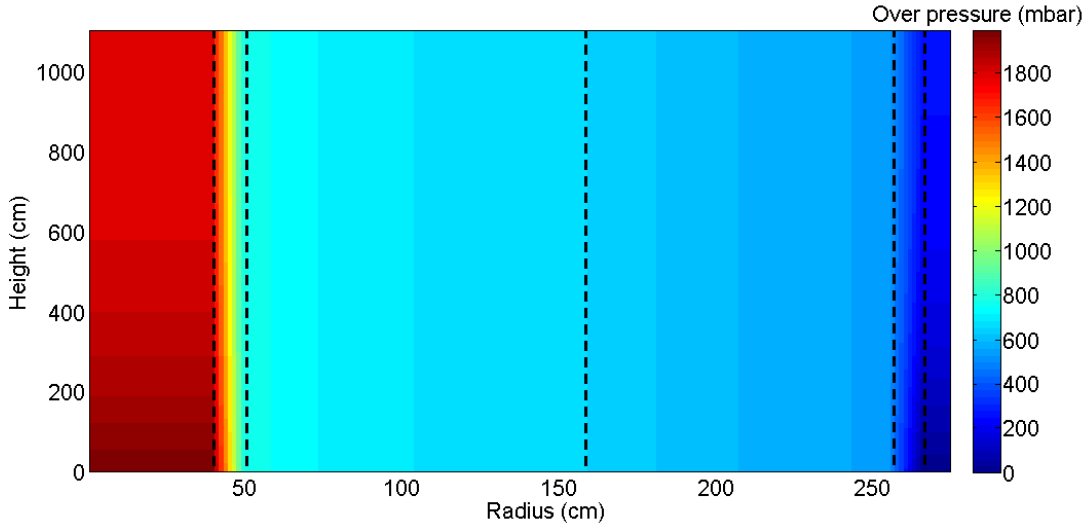

Figure 4.3: Pressure profile in a radially cooled reactor. The location of the inner reflector slits, driver/breeder interface and exterior reflector slits are visualized with dashed lines.

In table 4.1, the pressure drops over the core components are listed. The pressure drop over the slits depends amongst others on the total surface area the cross sections of the slit flow paths are allowed to occupy. The combined cross sectional area of the slits can be expressed as the total reflector area times the fraction of the flow paths (f_{area}). Furthermore, the velocity is expressed as function of the mass flow and the cross sectional area of the flow. Finally, the ratio of wetted perimeter to surface can be substituted:

$$A_{slits} = f_{area} A_{tot} \qquad v = \frac{\dot{m}}{\rho A_{slits}} \qquad \frac{P_w}{A} = \frac{2}{d_h} \tag{4.1}$$

Substituting these relations in equation 2.9, leads to the following relations:

$$\Delta p = \frac{fL}{d_h \rho} \left(\frac{\dot{m}}{A_{tot}} \right)^2 / f_{area}^2 \qquad f_{area} = \sqrt{\frac{1}{\Delta p} \frac{fL}{d_h \rho}} \left(\frac{\dot{m}}{A_{slits}} \right) \tag{4.2}$$

The ratio of mass flow rate over total reflector area is fixed for every core height, due to the required cooling of the core. Especially for the slits in the central reflector, the value of f_{area} is of major importance as it determines whether enough space will be available to place the control rod system at that location. The pressure drops listed in table 4.1 can be achieved by varying the slit occupation of the central reflector surface from 14% at the bottom, to 16% at the top of the reactor.

The occupation of a surface with 16% coolant flow slits is visualized in figure 4.4. In this figure, an area is generated where exactly 16% is occupied by circular coolant flow paths. As shown in the figure, enough space remains for the control rod guidance pipes, visualized in gray.

Combining the data from figures 4.3 and 4.4 and table 4.1, it is clearly possible to force sufficient coolant through the entire reactor, while the central reflector can also host the control rod system. The core dimensions ensure a relatively low pressure drop over the components surrounding the pebble bed. The resulting pressure drop over the core is about 20 millibar, where the pressure drop over an axially cooled core can be up to 1.13 bar.

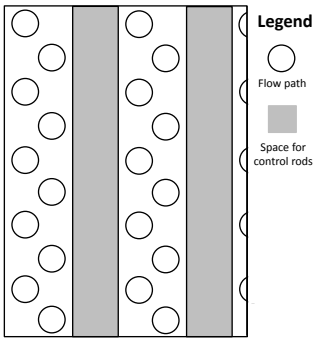

Figure 4.4: Visualization of a central reflector where 16% of the cross sectional area is occupied by coolant slits. It is clear that this percentage would allow the placement of control rod guidance tubes

Table 4.1: Pressure drop over the core components. The pressure drop over the slits is substantially higher than that over the other core compartments. This is a result of the flow regulation that must be achieved by this pressure drop, and of the limited dimensions of especially the central reflector

Inner coolant pipe:	2.1 mbar
Inner reflector slits:	10-12 mbar
Pebble bed: Driver zone:	1.2 mbar
Pebble bed: Breeder zone:	1.0 mbar
Outer reflector slits:	3-5.5 mbar
Outer coolant pipes:	2.5 mbar
Total:	20 mbar

4.2. STEADY STATE DALTON/THERMIX MODEL

In this section, the results for the converged steady state THERMIX and DALTON simulations will be discussed. The parameters of the model are shown in table 4.2. The power density and neutron flux calculated by DALTON will be discussed in the next subsections. After this, more attention will be paid to the coolant distribution and the accuracy of the flow regulation by the slit parameters. Finally, the temperature of the solid components will be treated in further detail.

4.2.1. POWER DENSITY

Table 4.2: Core parameters for the model with radial cooling

Thermal power	250 MW
Reflector radius	50 cm
Driver radius	125 cm
Breeder radius	176 cm
k_{eff}-value	1.0009
Mass flow rate	96 kg/s
System pressure	7 MPa

The shape of the power density in the radially cooled core is visualized in the left graph of figure 4.5. In this figure, the power density for an axially cooled core is given in the right graph for comparison. The power peak is located at the innermost region of the reactor, as is dictated by geometry, but it is not centered at the top of the reactor as in the axially cooled reactor. This is due to the cold coolant inflow. For an axially cooled core, this enters at the top of the core. Hence the temperature feedback increases reactivity at this location. For the radially cooled reactor, it flows in at the inner side of the core, and both geometry and temperature feedback enhance reactivity in the reactor center. This means that the power peak is axially centered. It might be suspected that this combination increases the intensity of the power peak, but it is actually more spread out, due to the sleekness of the core. The power density in the breeder zone is very low, with a sharp boundary between driver and breeder channel. The small amount of power in the breeder is concentrated at the bottom of the core, as in that part the pebbles have sufficient residence time in the reactor for breeding a reasonable amount of ura-

nium from the thorium. In the driver zone, the burn up effects are less influential, as the number of driver channel passages is 15 compared to 2 for the breeder channel.

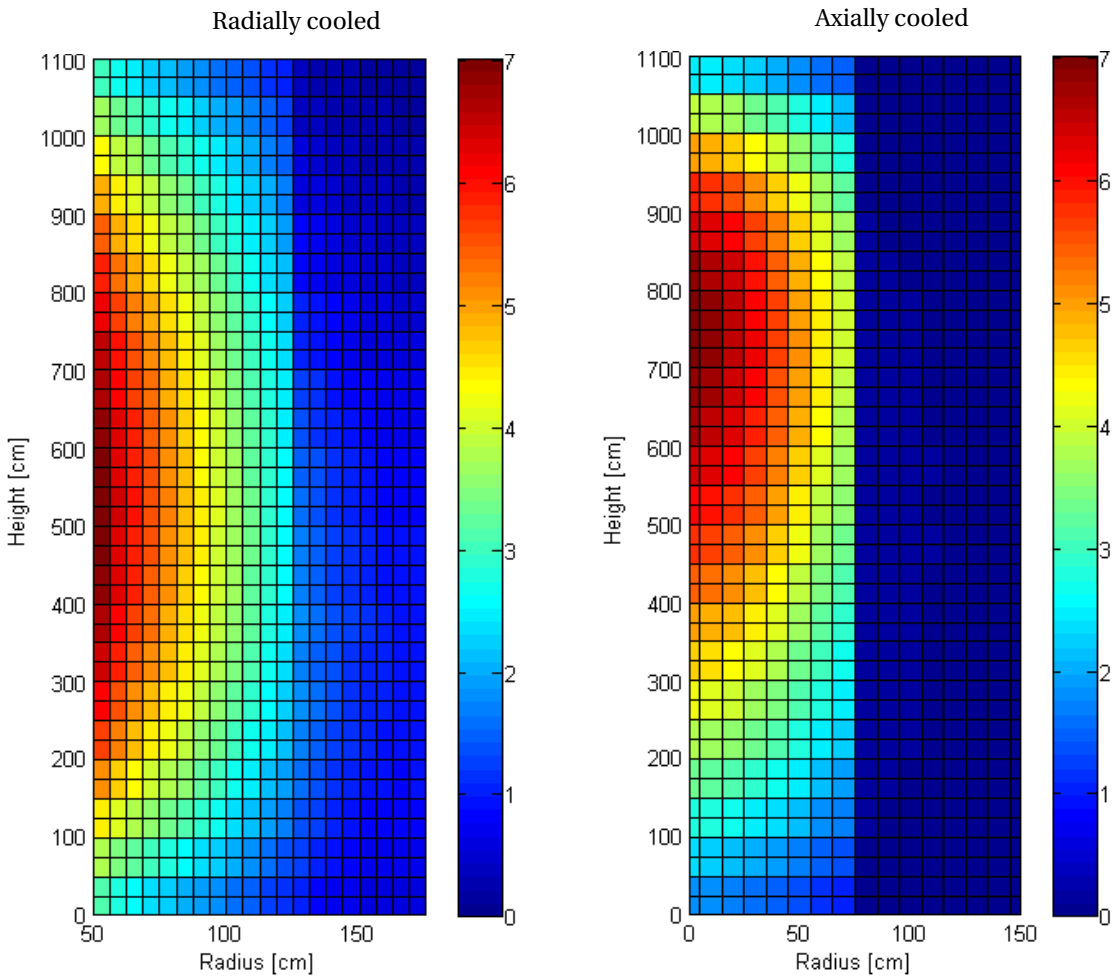

Figure 4.5: Power density for the radially cooled thorium breeder pebble bed reactor. For comparison, the power density of a system with axial cooling is provided.

4.2.2. NEUTRON FLUX

The neutron flux is calculated by DALTON in five energy groups, according to the boundaries given in table 3.1. The flux in the highest energy group is shown on the left graph in figure 4.6. The third group, that is epithermal, is shown in the central graph. The flux with the lowest energy is depicted on the right side of the figure. The flux in energy group two and four are omitted in this graph as their shapes are intermediate to the others. The neutrons scatter out of the fastest energy group due to the moderation with graphite. Therefore, the fast neutrons exist mainly in the high power density driver zone. Slowing down of the fast neutrons leads to epithermal neutrons, that are found in a larger part of the core. The slowest neutrons are found mainly in the central reflector region and the region directly adjacent to it. This is due to the large amount of graphite in this region, which provides a relatively high scattering to absorption macroscopic cross section ratio. In the calculation of these fluxes, it was assumed that the influence of the core composition outside the reflector regions was negligible. It can be seen that the neutron flux in the reflector zones surrounding the pebble bed is already almost negligible. This means that influences from positions further away have indeed insignificant influence on the core flux.

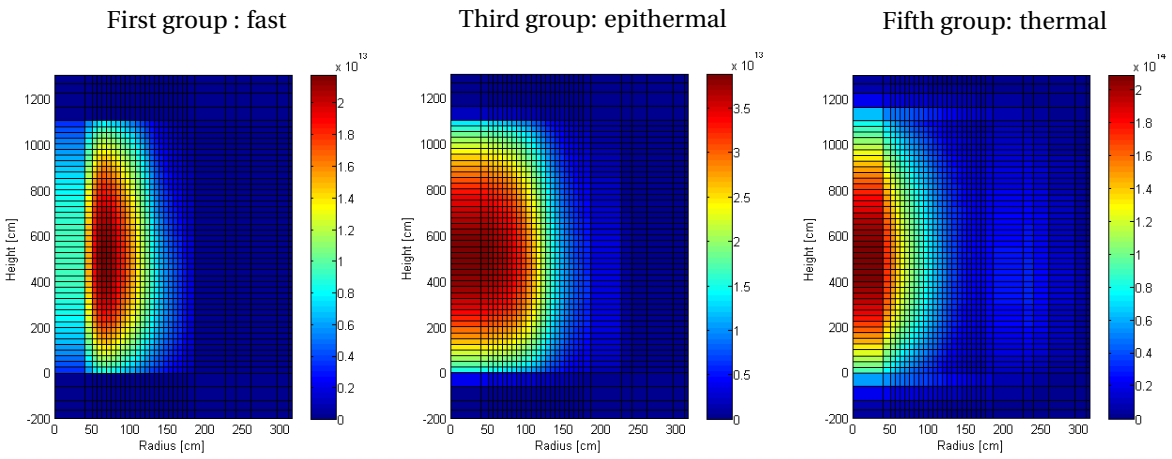

Figure 4.6: Neutron flux in several energy groups. The central reflector is visible as the relatively broad interval in the absolute center. Surrounding it is the finer mesh active pebble bed core.

4.2.3. COOLANT DISTRIBUTION

In figure 4.7, the coolant mass flow rate in radial direction is visualized for the core region. The radial mass flow that traverses the center of the core first decreases and then increases, while at the top and bottom, it first increases and then decreases. This is explained as follows.

Fresh coolant is injected in the core through the horizontal slits in the central reflector. Then it flows through the pebble bed and expands due to the added heat. The power density is higher in the centre of the core than at the top and bottom. This causes a mild divergence around the power peak, that has to be accounted for by adjusting the inner slit parameters. When the coolant reaches the outside of the core, the mass flow converges again. This is due to the axial variation in the pressure drop over the outer slits, which is very high at the top and bottom of the core. This is explained by the divergence around the hot center region.

The average deviation of the radial mass flow from the mean radial mass flow is less than 0.4%,

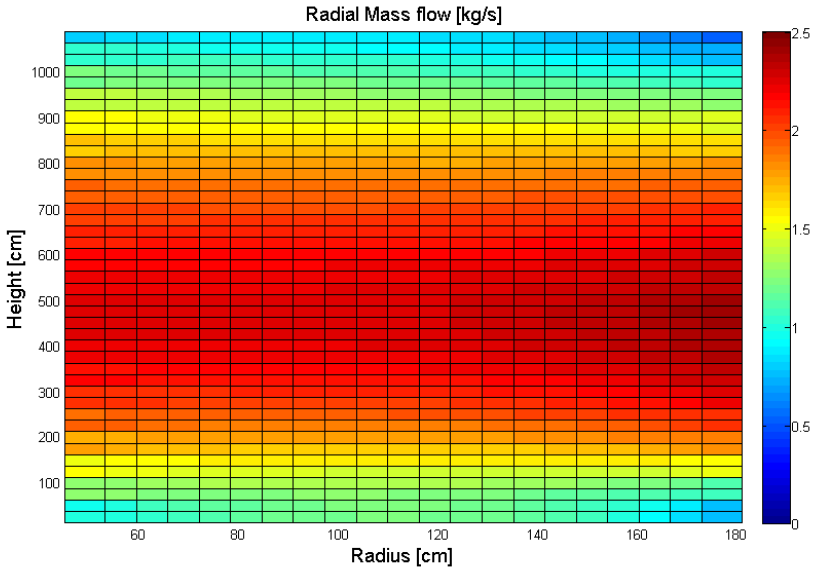

Figure 4.7: Radial mass flow in [kg/s]. The flow is almost radially invariant, except for an increase in mass flow in the exterior center. This is a result of compensating for the divergence around the central power peak.

hence the divergence effect can be corrected for sufficiently. The coolant is able to cool all parts of the reactor effectively, as can be verified by the coolant temperature distribution, which is visualized the right graph of figure 4.9.

It can be seen that the deviations in the mass flow do not create large variations in the axial temperatures. The exact outflow temperatures are visualized in figure 4.8. The temperatures are consistently about 10 K above the core reactor outflow temperature of 750 °C. This is due to the energy that is transferred to the risers, preheating the fresh coolant. Oscillations around this average value arise at the bottom of the core (0-200cm), because the slit parameters are defined in spatial intervals that each contain two flow intervals. The low flow rate in this region makes that this constraint causes relatively large outflow temperature oscillations. At the top of the core, the outflow temperature is relatively low. This is due to the combined effect of the nearby riser and upper plenum, that effectively cools the solids in this region.

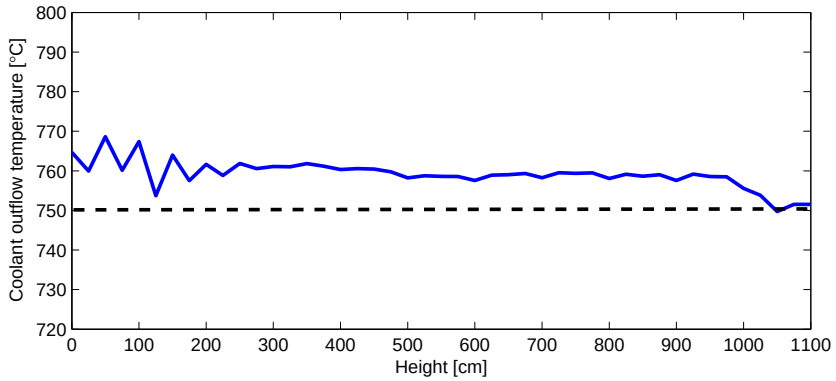

Figure 4.8: Axial variation in coolant temperature at the core outflow, which is located at 176 cm radius.

The variations are relatively small and have negligible effect on the thermal efficiency. The variations are erased when the coolant mixes in the vertical outflow pipes. An average coolant outflow temperature of 750 °C can be reached while the local gas temperature is maximal 768 °C. Hence the maximum fuel temperature is not significantly influenced by the coolant temperature variations. The coolant effectively transports the thermal energy out of the system, with low heat transfer through the surrounding layers to the boundaries, as will be treated in the next section.

4.2.4. SOLID COMPONENTS TEMPERATURES

The steady state solid temperature profile of the core is also depicted in figure 4.9. In the packed bed, the graphite temperature follows the trend of the helium temperature, yet it is slightly higher due to the temperature jump for heat transfer from the solid to the coolant. In the surrounding areas, the temperature is lower, but still reasonably high, especially at the location around the hot helium outflow. The fresh coolant flowing through the riser channels cools the side of the reactor, which significantly lowers the solid temperature there, especially in the uppermost region of the vertical outflow pipes. The carbon brick provides very efficient thermal resistance, hence the temperatures of the layers beyond this are very low. The thermal properties of this layer and other thermal insulating layers, as the top and bottom insulator and the various gaps, lead to a thermal leakage at the boundaries of only 0.14% of the total thermal power. The central reflector is constantly cooled by fresh helium, and reaches temperatures only a few degrees above the cold helium inlet temperature. This makes it possible to place the control rod system here, as the control rods can easily resists these temperatures [16]. The maximum steady state temperatures of various reactor components are given in table 4.3. The temperature of the metallic internals and the RPV do not exceed 350°C, which is the maximum temperature for safe operation defined for the HTR-PM design [6].

Table 4.3: Maximal steady state temperature per reactor component.

Component:	Central reflector	Exterior reflector	Carbon Brick	Metallic Internals	RPV
Temperature:	256°C	714°C	526°C	336°C	219°C

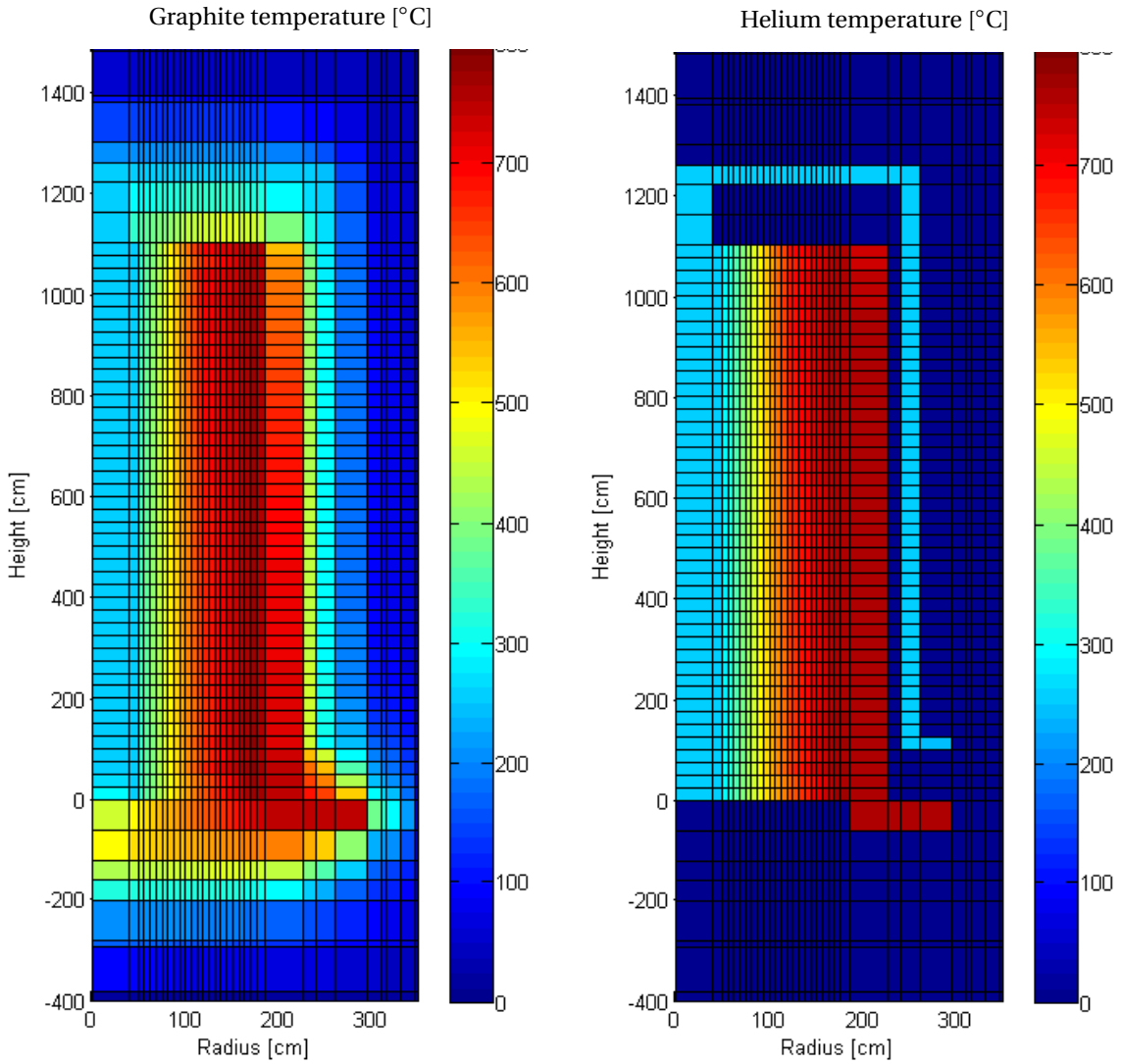

Figure 4.9: Temperature profiles of the radially cooled reactor core for both the solid parts (graphite) and the coolant (helium).

4.3. TRANSIENT SCENARIOS IN THE RADIALLY COOLED CORE

The steady state results were used as initial condition for the simulation of the time dependent scenarios. Both pressurized and depressurized loss of forced cooling (PLOFC and DLOFC) scenarios were considered. The results of these simulations will be treated in the following section. Special attention was given to the effect of convection and core heterogeneity in DLOFC scenarios. The results of this will be treated in the section thereafter.

4.3.1. LOSS OF FORCED COOLING INCIDENTS

Starting from the steady state conditions, simulations were performed of loss of forced cooling incidents with immediate SCRAM. A parameter of great importance is the maximum fuel temperature, as it determines whether there is a possible release of radionuclides from the pebbles. Effective retainment of fission products is assured for fuel kernel temperatures below 1600°C [33]. The maximum fuel temperatures for both a pressurized as a depressurized incident with SCRAM are given in figure 4.10. It can be seen that the maximal allowable fuel temperature is not reached, with a

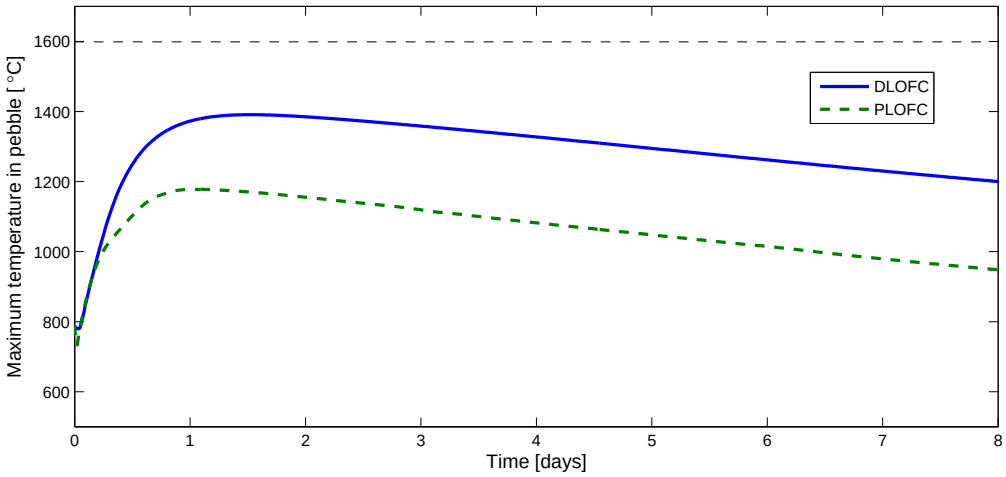

Figure 4.10: Maximal fuel temperature reached in DLOFC and PLOFC incidents in the radially cooled core. The maximal safe fuel temperature of 1600 °C is depicted with a dashed line.

relatively large margin. This shows that for this reactor design, passive mechanisms provide sufficient cooling. It can be seen that a DLOFC incident yields a higher maximum temperature than a PLOFC incident. This is expected, as the contribution of natural convection is significantly lower in this case. The shape of the DLOFC temperature curve is similar to that found for the HTR-PM [6], which is shown in appendix A. The difference between the PLOFC scenarios for the HTR-PM and the radially cooled reactor is larger. This means that the effect of natural circulation is different in

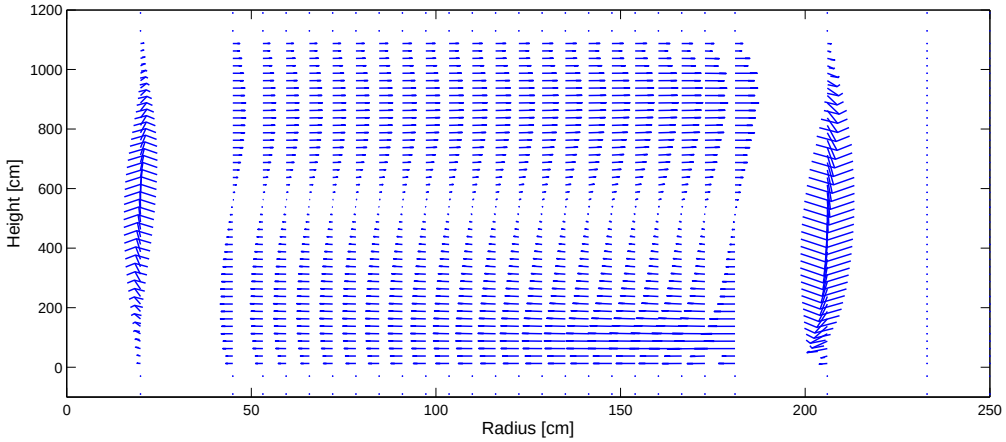

Figure 4.11: Core mass flow vectors during a PLOFC incident after 4 days since start of the transient. The coolant travels upwards through the central reflector, outwards through the upper part of the core, downwards through the exterior reflectors and inwards through the lower part of the core. The pebble bed flow is purely radial.

radially cooled systems than in axially cooled ones. The HTR-PM PLOFC curve follows the corresponding DLOFC curve till roughly 4 hours, after which it drops rapidly and takes on a equilibrium value, which means a sharp peak arises just after the start of the transient. This could be due to the fact that at the start of the transient, the hot helium in the center is being pushed upwards, right into the power density peak. This would result in a raise of temperature at the beginning, and a sharp reduction later, as the circulation provides effective heat removal. In the radially cooled design, the power density is more spread out, and the peak is located in the center rather than at the top. This means that the hot helium is transported out of the power density power peak faster. This would explain the fact that the maximum PLOFC temperature for this design is subsequently lower than the maximum DLOFC temperature, and does not have the sharp peak that is typical for PLOFC incidents in an axially cooled reactor. The natural convection induces a mass flow through the core. The shape of this mass flow, at four days after the start of the transient, is visualized in figure 4.11. It can be seen that the vertical flow pipes in both the central as the exterior reflector facilitate a large axial mass flow. In the pebble bed, the mass flow is almost purely radial. This can be explained by the PLOFC temperature profile, which is visualized in figure 4.12. In the central reflector, the temperature is high, hence the coolant rises. In the exterior coolant flow pipes, the helium cools down, hence it drops. The temperature profile for a DLOFC incident is also given in figure 4.12. As

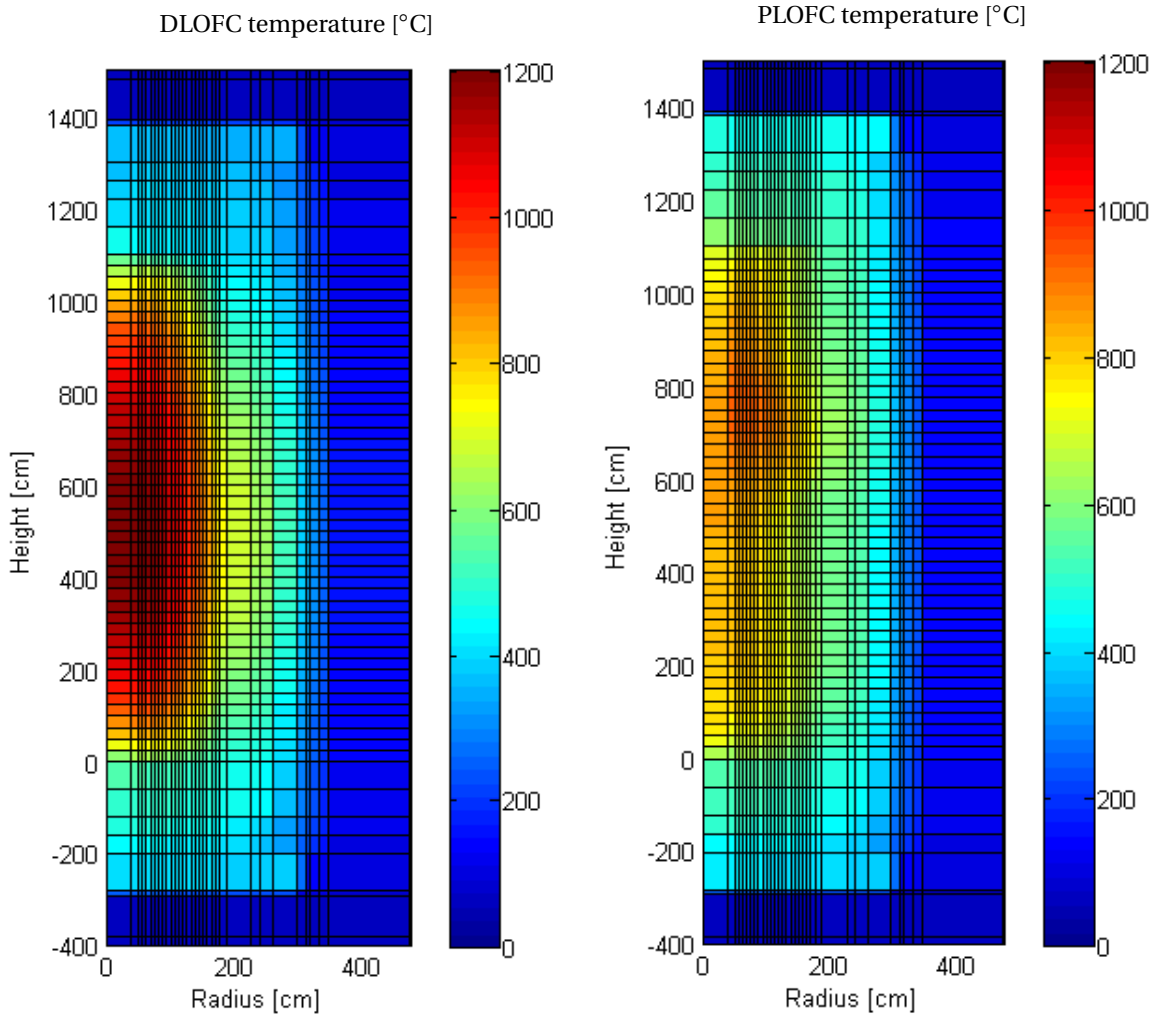

Figure 4.12: Graphite temperature profiles of the core for both DLOFC and PLOFC incidents.

the influence of convection is negligible, the temperature is mainly determined by conduction and radiation. This leads to a temperature that decreases monotone from the centre of the core. The core temperature is much lower in the PLOFC case, due to the influence of convection. However the convection increases heat transport to the outer reflector layers, which means that the temperature, especially in the upper part of these layers, is actually higher than in the DLOFC case.

4.3.2. INFLUENCE OF CONVECTION AND HETEROGENEITY ON DLOFC

Convection has a large influence in PLOFC scenarios, as can be seen from the differences between PLOFC and DLOFC maximum fuel temperatures. In a DLOFC incident however, the majority of the helium in the core escapes from the primary circuit during the depressurization. This means that natural convection is limited, as the volumetric thermal capacity (ρc_p) associated with atmospheric pressure is almost negligible. To quantify the influence of convection in DLOFC scenarios, calculations were performed with the convective part omitted. The results are compared to DLOFC simulations with convection in figure 4.13. It can be seen that convection has indeed a small, yet noticeable influence on the maximum fuel temperatures in DLOFC incidents. It does add heat removal capability, but not enough to change the maximum temperatures by more than a few degrees. In this figure, the effects resulting from pebble inhomogeneity are also visualized. A homogenous pebble means that a uniform temperature profile over the pebble radius is assumed. In the heterogenous pebble case, the temperature is calculated separately for a multiple of pebble shells. In coupled calculations, pebble temperature heterogeneity must always be accounted for, as it is of major importance for the accuracy of the cross section interpolation results to use correct fuel temperatures. Exact temperatures are also important for another reason. For a pebble with a large temperature gradient, the average temperature can be well below 1600 degrees, while the center is hotter, leading to a potential release of radionuclides. So, a significant safety failure could stay undetected. In figure 4.13, It can be seen that the difference between the highest fuel temperature and the average solid temperature is significant at the start of the transient. This is because at that moment, the power equals the normal operating power, and the pebble conductivity is not high enough for heat removal without a significant temperature gradient. Assuming constant thermal conductivity of the pebble, the temperature difference is proportional to the power density. When the transient

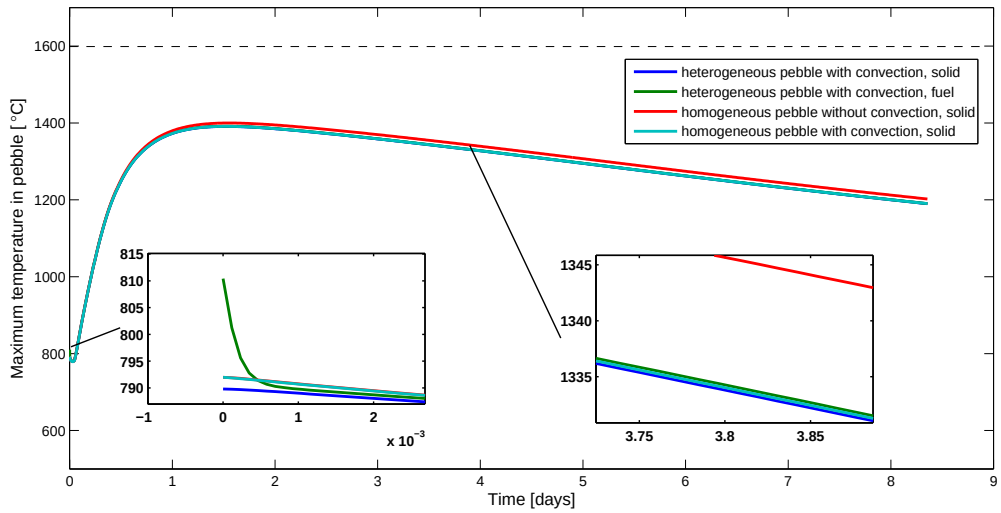

Figure 4.13: Effects on maximum temperature of convection and core heterogeneity. Only convection creates a relatively large difference of about 8°C, for the heterogenous model, the maximum fuel temperature is around 1°C above its surface temperature. The averaged temperature of the homogenous pebble is between them.

proceeds, the power drops fast, and a minimal temperature gradient is sufficient to remove this low decay power. Hence the difference between temperatures in the homogenous (averaged) pebble simulations and the highest fuel temperature in the heterogenous case is not significant any longer. It can be concluded from these results that it is valid to use homogenous pebble temperature calculations and omit convection in DLOFC simulations.

4.4. REVERSING THE COOLANT FLOW DIRECTION

So far in this research, the radial coolant flow direction was from the central reflector to the exterior slits and pipes. This flow direction will henceforth be denoted as "outward flow". The opposite flow direction can also be adopted, where the coolant flows from the outside of the core to the inside. This concept is used as a design variation in this research. The effects of applying this flow direction, which will be called "inward flow" from now on, are discussed in the following section.

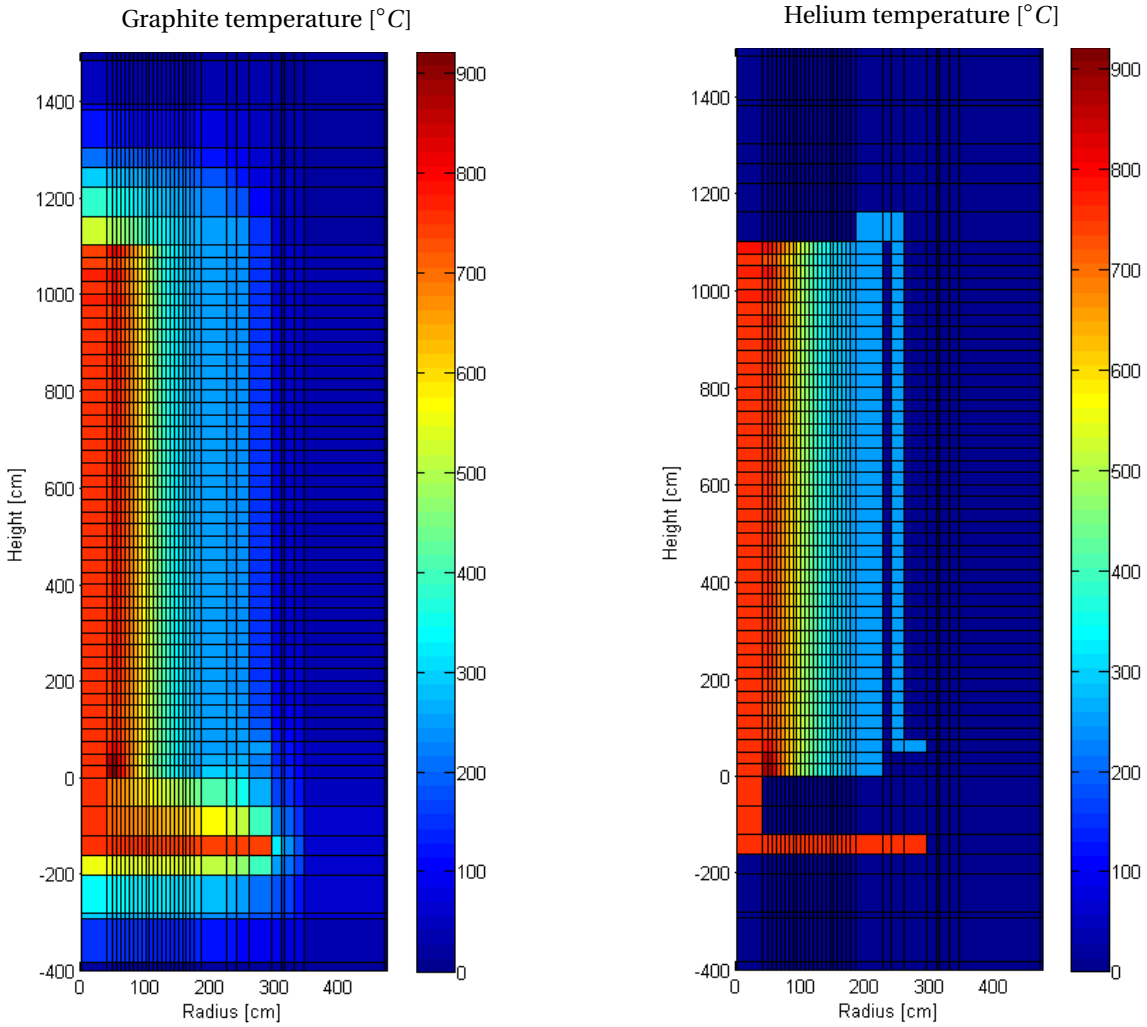

Figure 4.14: Steady state solid and coolant temperature profiles for the reversed flow model.

4.4.1. TEMPERATURE DISTRIBUTION

When the coolant direction is reversed, the helium temperature profile in the reactor core will be mirrored. An outward flow reactor has a relatively cool zone in the center of the reactor, and the hottest spot at the outside of the pebble bed as depicted previously in figure 4.9. When inward flow is adopted, the center of the reactor becomes the hottest region, as depicted in figure 4.14. In the center bottom corner of the core, around r=50cm and z=25cm, a small hot spot arises. It is assumed to be a numerical error due to the 90 degree change in coolant flow direction at this point, from the purely horizontal flow slit area to the purely vertical central tube.

The first obvious drawback of an inward cooled system is that it is no longer possible to place a standard control rod system in the central reflector. The steady state temperature of this location is to high to allow the placement of such a system. This means that a special control rod system with a higher allowable operating temperature has to be used, which is probably more expensive. Or, the control rods have to be placed in a different location, which is a major drawback since the placement of control rods in the central reflector is one of the largest benefits for the radially cooled design.

A second drawback of inward cooling is that the hottest coolant cools the part of the reactor with the highest power density, while the cold coolant is used to cool the breeder, which has a very low power density. This is opposite from the outward flow design, where the fresh coolant cools the driver zone, and when it is heated it also cools the breeder zone. The temperature jump between pebble and coolant is proportional with the power density, hence it is bigger in the driver zone than in the breeder zone. This is visualized in figure 4.15, where the difference between graphite and helium temperature at central core height is given as function of the radius. In the outward flow scenario, the effects of the large temperature jump in the driver zone are mitigated as this is a relatively cool zone. The highest temperatures occur in the breeder zone, where the low power density decreases the temperature jump. In the inward cooled case however, the driver is the hottest zone, and the jump causes graphite temperatures up to 70°C higher than the helium outflow temperature, which induces worse initial conditions for transient scenarios.

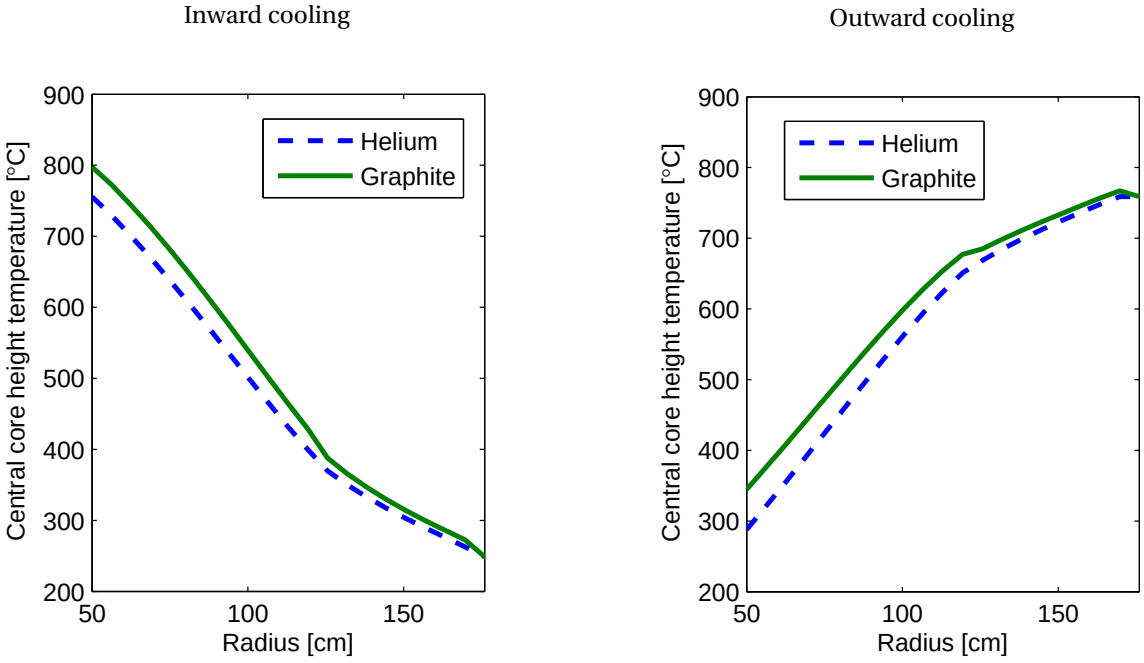

Figure 4.15: Centre core graphite and helium temperatures for radially cooled thorium breeder pebble bed reactors with different flow directions

4.4.2. POWER DENSITY

The effects of reversing the coolant flow direction on the power density are visualized in figure 4.16. For easy comparison, the power density for outward flow, as depicted figure 4.5, is also given. As can be seen, the power density is less peaked and shifted more to the exterior side for the inward flow case. This occurs because the temperature feedback now enhances reactivity in the exterior of the core, and diminishes it in the center. This reduces the power peaking in the center, that is normal due to the geometry. Reversing the coolant flow direction also has a reactivity effect. A k_{eff} value of 0.983 was found for the system with inward flow, which is 0.018 lower than the k_{eff} found in the system with outward flow. This could be due to an increase in the neutron leakage. This negative influence on the reactivity might alter the breeder ratio for this design. However, more elaborate burn up calculations have to be performed in order to quantify this accurately. The larger spread in the power density could be an advantage for transient scenarios. As the power density is located more to the exterior of the core, it should be easier to remove the decay heat.

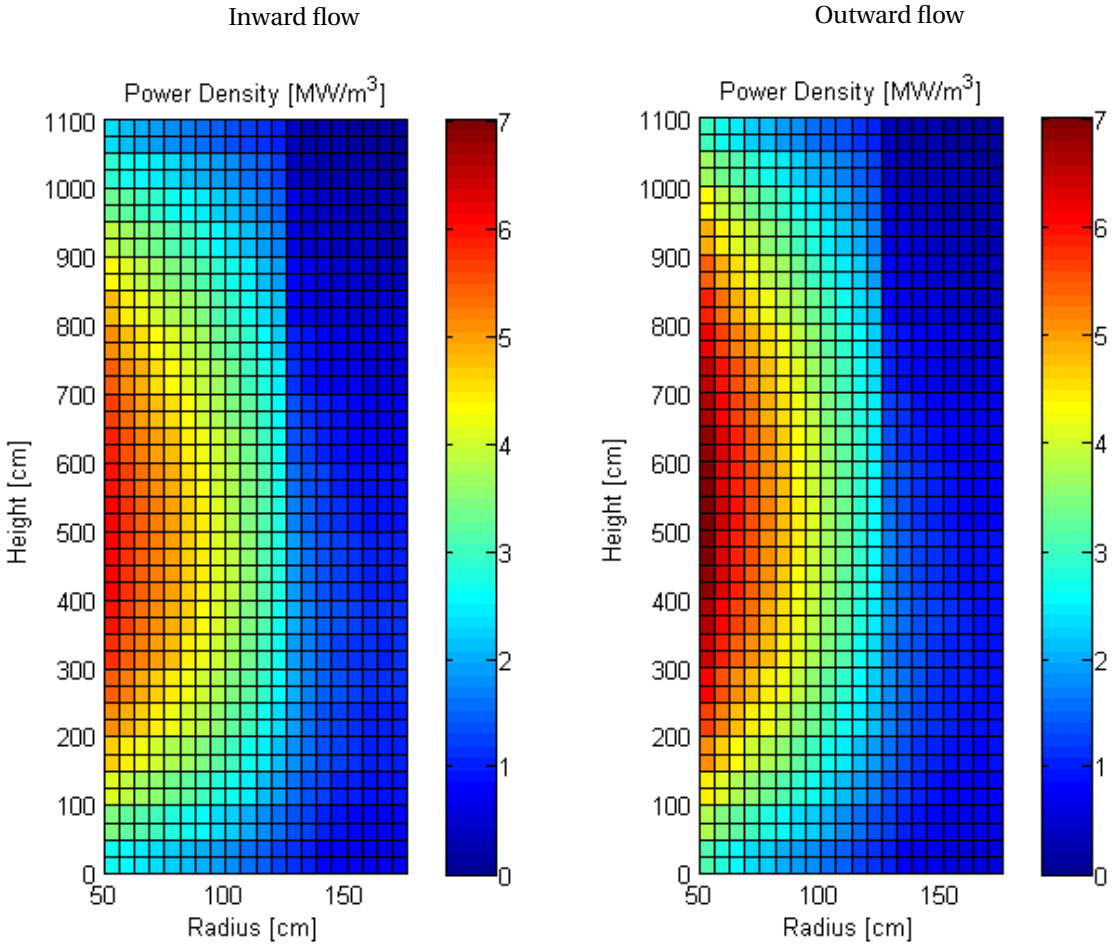

Figure 4.16: Power density for radially cooled thorium breeder pebble bed reactors with different flow directions

4.4.3. TRANSIENTS

In order to investigate the effects of reversing the coolant direction on the maximum fuel temperatures reached in transient scenarios, time dependent DLOFC scenarios were simulated for an inward cooled reactor. The PLOFC incident was not taken into account, as the DLOFC case gives consistently higher temperatures, and can be treated as the worst case scenario. The maximum fuel

temperatures are visualized in figure 4.17. For easy comparison, the curve for outward cooling is shown again. The maximum fuel temperature of the model with inward flow direction is initially higher, due to the larger temperature gap between driver coolant and pebble surface. However, with the proceeding of time it rises slower than the inward flow temperature, and when both fuel temperatures are at their maximum, it is lower by about 60°C. This is explained by the shift of the power density to the exterior of the core, which makes heat removal easier. The lower maximum fuel temperature is an advantage of adopting inward cooling. However, the temperature margin is already sufficient for the reactor with outward flow direction, and the drawbacks of reversing the coolant direction are more important than its lower maximum temperature. Only in a system with smaller temperature margins, for example a reactor operating at higher power, reversing the coolant flow direction becomes attractive.

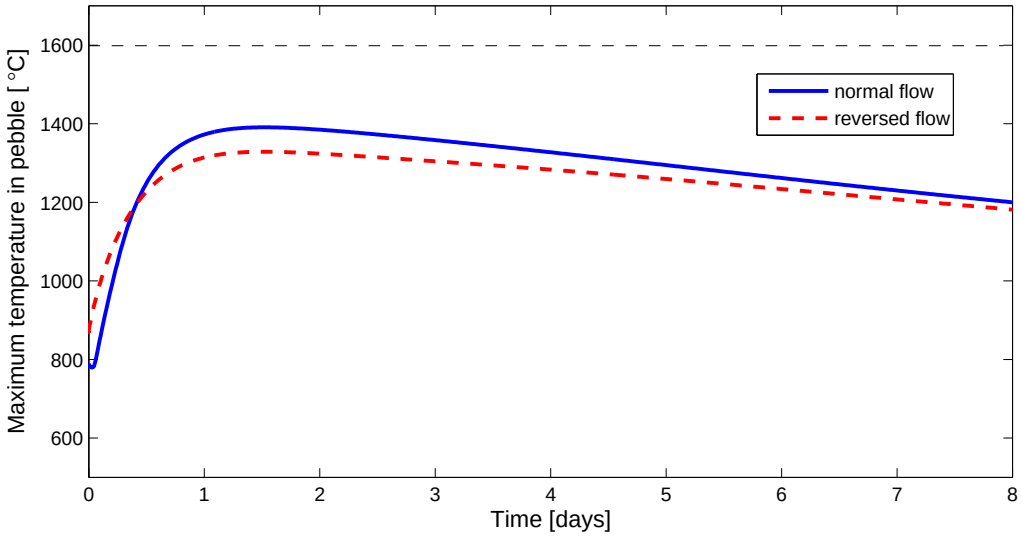

Figure 4.17: Maximal fuel temperature in depressurized loss of forced cooling scenarios for both the normal (outward) and the reversed (inward) flow direction systems. The reversed flow maximum temperature is higher at the beginning of the transient, but reaches a lower maximum.

5

CONCLUSIONS

5.1. MAIN CONCLUSIONS

The main research question was whether it is feasible to radially cool a thorium breeder pebble bed type HTR, within the required safety and economical constraints. Various aspects of the radially cooled core were investigated with the coupled THERMIX / DALTON code, focussing on the steady state behaviour. The conclusions on this investigation will be treated in the following section. Subsequently it will be compared to the axially cooled core, on basis of two corresponding MATLAB models. Finally conclusions on the safety of the reactor will be examined, focussing on the transient behaviour calculated with THERMIX in time dependent mode.

FEASIBILITY OF A RADIALLY COOLED THORIUM BREEDER HTR

Pressure The pressure profile determines if there is sufficient mass flow rate to cool each core region. The average deviation of the radial mass flow from the mean radial mass flow is 0.4 percent. Some divergence around the power peak arises but this is accounted for in the slit dimensions. The axial coolant outflow temperature variations are relatively small. The deviation is less than 10°C around the average value, which is almost 10°C above the core final outlet temperature. This is due to preheating of the coolant in the riser channels. This mass flow distribution is achieved with a total core pressure drop of 38 millibar. This is significantly lower than in axially cooled pebble bed cores, where the pressure drop is typically over 1 bar.

Control rods The placement of the control rod system in the central reflector is very well feasible. The coolant flow slits cause a maximum of 16% of central reflector wall penetration. This leaves enough space for the placement of the control rod system, without compromising the reflector structural integrity. In the outward cooled core, the central reflector temperature is only a few degrees above the coolant inlet temperature of 250°C. This means that the fresh coolant cools the central reflector sufficiently for the placement of a standard control rod system. For the inward cooled core, central reflector temperatures well above the helium outlet temperature of 750°C are reached. If a control rod system is placed here, it must be resistant to these high temperatures.

Solid temperatures The maximum fuel and average pebble temperature are 781°C and 778°C respectively for the outward cooled core. They are relatively close to each other, since the hottest part of the reactor in this case is the breeder zone, which has a very low power production. For the inward cooled case, the hottest part of the reactor is the driver zone, which has the highest power density. In this case, the maximum fuel and average pebble temperatures are higher and further apart, 1038°C and 827°C respectively. In both cases, the carbon brick layer provides sufficient heat insulation. This means that the metallic internals and reactor pressure vessel do not exceed the limit of 350°C,

which is the safety limit for steady state operation defined for the HTR-PM. For efficient electrical power generation, the thermal leakage form the core needs to be low. The insulating layers at the top and bottom of the core further decrease the heat transport in the axial direction. This makes the thermal leakage over the top and bottom boundary negligible. In the radial direction, complete thermal insulation is not possible, as the heat transport towards the water cooled panel is of major importance for safety in LOFC incidents. Still the forced cooling effectively removes the heat, leading to a thermal energy leakage to the boundaries of less than 0.14% of the total thermal power.

Neutronics The power density for the radially cooled core is axially centered, and has a large axial and radial spread, especially for the inward cooled core. The thermal flux is concentrated in and around the central reflector. The fast flux is located at the power density peak, since these neutrons are created only in fission events, and rapidly scatter to a lower energy group due to the graphite moderation. Epithermal neutrons are found in both these regions. Excluding zones outside of the exterior reflectors from the computational domain is a valid simplification as the flux there is insignificant.

COMPARISON WITH AXIAL COOLING

From the comparison with the THERMIX reference case, it is verified that the relations used in the MATLAB models produce realistic results. These models were used to investigate whether radial cooling could solve three major problems of axially cooled thorium breeder HTRs, being helium thermal mixing, high pressure drop, and reactivity control. It was found that all of these problems were effectively solved by the placement of a central reflector and adopting radial cooling.

Helium thermal mixing The hot and cold helium mixing between driver and breeder channel affects the outflow temperature. When the outlet coolant is mixed, the temperature drops from 750°C for the driver outlet to 450°C for the average outlet. The Carnot maximal theoretical achievable thermal efficiency [34] would decrease from 48.9% to 27.6%. Clearly this is an intolerable loss of efficiency.

This means that the breeder channel coolant has to be separated and pumped through the system once more. The already relatively high pressure drop would then almost double, as the majority of the coolant is not hot enough for direct energy conversion. In the radially cooled core, these kind of effects do not occur, as the coolant traverses both the driver and breeder channel, leading to a uniform coolant outflow temperature of 750°C.

Pressure drop The pressure drop over the axially cooled core is around 1.2 bar. The pressure drop over the radially cooled core is substantially lower, approximately 38 millibar. This means that the required pumping power is reduced from 1.7 MW to 54 kW, according to equation 2.7.

Reactivity control The central reflector required for radial cooling not only provides extra moderation in the core centre, but is also an excellent host for the control rod guide tubes. This region is constantly cooled by fresh helium in the outward cooled design. In the axially cooled core design, there is no central reflector. This means that either the control rods have to be driven through the pebble bed, which is unfavourable due to pebble damage, or placed in the exterior reflector. The positioning of control rods in the exterior reflectors is problematic due to the low flux, which is caused by the low power breeder zone.

REACTOR SAFETY

In terms of reactor safety, attention focussed on the maximum fuel temperatures in loss of forced cooling scenarios with SCRAM. Furthermore the effects of natural convection in these scenarios was investigated.

Maximum fuel temperatures It was found that the proposed reactor design is passively safe in both PLOFC and DLOFC incidents with SCRAM. The maximum fuel temperatures are 1391°C for a DLOFC incident, and 1178°C for a PLOFC incident. These values leave a wide margin to the maximal radioactivity retainment temperature of 1600°C. In principle, this means that there is space for design variations to optimize other parameters. For example, it is possible to increase the core radius or operate the reactor at a higher power. Furthermore, it was found that pebble heterogeneity had no significant influence on the fuel temperatures during the transients. This is due to the low power production during the transient, that can be removed without a large temperature difference over the pebble.

Influence of convection Convection has negligible influence on the maximum temperature that is reached in a DLOFC incident. For this type of incident, the convective part of the simulation can be omitted, which simplifies the calculation and substantially decreases computation time. This makes it possible to check worst case scenario temperatures on the fly while optimizing core parameters.

In a PLOFC incident, the natural convection significantly lowers the core temperature. It is further noticed that the central and exterior vertical coolant flow pipes in the radially cooled core provide excellent flow paths for the circulation. It can be seen that almost all vertical flow is through these pipes, while the helium flows radially inward through the bottom half of the core, and radially outward through the upper half. This resembles a singular concentric Rayleigh-Bernard cell.

5.2. DISCUSSIONS

This section focusses on two main items. It discusses which coolant flow direction is favourable. Furthermore, the effects related to transient reactivity control are treated.

COOLANT FLOW DIRECTION

Central reflector temperature In the outward flow steady state case, the central reflector is constantly cooled by fresh helium and reaches a maximum temperature of only 256°C. For this reason it is a very suitable location to place a standard control rod system. In the inward cooled design, the steady state temperature of the central reflector reaches up to 820°C. A control rod system able to withstand these temperatures is possible. For example, a control rod consisting of a sleeve and spine of Incoloy 800, containing carbon encapsulated boron carbide has been proposed [16]. However, such a system is probably more complex in manufacture and maintenance, and more costly.

Power density For the inwardly cooled core, the power density is more spread out in the radial direction than it is for the outwardly cooled core. This corresponds to the larger spread of the flux, which is due to the temperature feedback of the fresh coolant, that enhances reactivity in the colder exterior side of the core. The larger spread in flux causes an increase in neutron leakage from the core, which induces a negative reactivity that reduces the k_{eff}-value with 0.018. A lower reactivity will have an effect on the breeding ratio. However, this cannot be determined without full burn up calculations.

Influence on transients The effects of the coolant flow direction on the maximum fuel temperature in a DLOFC incident where investigated in this research. This incident type was chosen because it is the worst case scenario. It was found that, compared to the outward cooled system, the initial maximum temperature is 70°C higher in the inward cooled system. This is due to the steady state temperatures, as is depicted in more detail in section 4.4.1. The rise in temperature in the inward cooled case is slower however, and it reaches a peak value of 1327°C, which is 65°C lower than the

temperature reached in the outward cooled case. Clearly, this effect is caused by the larger spread and lower peak of the power density, which facilitates easier heat removal.

Conclusion The maximal temperature reached in a DLOFC incident is lower for inward flow. However, the margin is already high enough for outward flow, hence the advantage is not extremely large. The criticality control is more troublesome for inward flow, due to temperature constraints on the control rod system. Hence outward flow is more favourable for this design. Only when the maximum temperature becomes an issue, for example when a higher power density or a larger core radius is considered, does inward cooling become a feasible design option.

REACTIVITY CONTROL IN TRANSIENTS

Rod structural integrity When a LOFC transient develops, the temperature in the central reflector becomes very high, both in the inward and outward cooled case. Even when the SCRAM successfully stops the chain reaction, the thermal degradation of the control rods means that it probably has to be replaced after a serious incident. This leads to higher costs, yet this is not a very serious drawback as the occurrence of such severe incidents is very rare. Also, the cost of control rod system replacement would be negligible compared to other costs. A more serious concern is whether the control rods can manage to maintain their reactivity worth at these high temperatures. Incoloy 800 undergoes significant creep above 1100°C, and melts at 1370°C. This means that it can not safely sustain the temperatures reached for this design, and that other systems are needed for transient criticality control.

Other emergency systems To ensure sub-criticality during the transients, an extra emergency shutdown system has to be installed. This can be the application of small ceramic neutron absorbing balls, called a KLAK-system [35]. Boron migration out of these boronated graphite spheres will not occur below 2800°C. Hence, this system can safely sustain the temperatures reached in transients. Two separate reactivity control systems are needed anyway due to legislation, so the control rod system would serve for control during normal operational conditions, and the KLAK-system for emergency situations.

5.3. RECOMMENDATIONS

REACTOR DESIGN

Thorium breeder HTR The thorium breeder HTR has a lot of advantages over current reactor designs. Thorium natural resources are less scarce than the uranium ones, the waste contains less higher actinides, and the proliferation risks are lower. The HTR provides for an inherently safe reactor with high thermal efficiency. The problems involving helium mixing, high pressure drop and reactivity control are all solved with the placement of a central reflector and the adoption of radial cooling, as was concluded in section 5.1.

Radial cooling specifics In case of a radially cooled core, the outward cooling direction is considered as most favourable. The coolant should flow into the central reflector at the top of the core, and out of the exterior pipes at the bottom. This way, gravity partially cancels the tube pressure drop, allowing for easier flow control with less strict requirements on the slit dimensions. This coolant flow design requires the presence of riser channels. The coolant flowing through the risers cools the side of the reactor, while the upper plenum cools the top. If necessary, an extra cooling loop can be put under the core, to achieve cooling of the material in this location.

FUTURE WORK

Burn up calculations For this research, the nuclide concentrations of an axially cooled thorium breeder HTR were used as a basis for the cross section preparation. Although it is reasonable to assume that there are no substantial differences in equilibrium concentrations for systems with altered cooling direction, the placement of a central reflector creates a large change in geometry. Hence, the reactivity in this core is not exact. Simulations including burn up calculations of a radially cooled system with central reflector have to be performed in order to find the exact reactivity and breeding ratio. Including burn up calculations can also give more information about the effect on breeding of the reactivity change related to an inward versus an outward coolant flow direction.

Reactor lifetime slit dimensions For this research, only the equilibrium core was simulated. The freshly fuelled start up core will have a different power distribution than the equilibrium one. Also, the end of life operation will alter the power distribution. Axial power density variations lead to altered coolant mass flow requirements. The slit dimensions, that regulate the mass flow rate distribution, can probably not be varied during the reactor life. This means that differences in the outflow temperature arise. It would be interesting to see to what extend these effects will occur, by coupling the existing thermal hydraulics / neutronics code to burn up calculations for the total reactor lifetime.

Transients without SCRAM In this research, the occurrence of a SCRAM was assumed at the start of each loss of forced cooling accident. That is reasonable, as an event with long-term failure to SCRAM the reactor is extremely unlikely [28]. However, before a nuclear reactor can be called inherently safe, its criticality control needs to rely on purely passive mechanisms, such as temperature feedback, and not on control rod insertion, which is still considered an active system. Loss of forced cooling incidents without SCRAM can only be simulated if the neutronics/thermal hydraulics coupling is continued in the time dependent mode. This was not the case in this research, hence including it is a recommendation for future research.

Central reflector RHRS An advanced pebble bed high temperature reactor design where the Residual Heat Removal System (RHRS) is placed in a central reflector has been proposed [36]. In this research, the same RHRS as in the HTR-PM was used. Hence all decay heat had to be transported to the water cooled panel at the radial boundary of the reactor. Placing the RHRS in the central reflector could substantially decrease the maximum fuel temperatures reached in loss of forced cooling scenarios. Also, there would be less restrictions on the radial heat conductivity, which might lead to lower thermal energy losses. The central reflector in the radially cooled thorium breeder already functions as a vertical flow pipe, and contains the slits and reactivity control systems. This means that the potential space available for a RHRS is very limited. However, since the decay heat removal is easier, the central reflector radius could be increased. Hence, the feasibility of adding a RHRS to the central reflector might be an interesting research topic.

BIBLIOGRAPHY

[1] D.E. Shropshire and J.S. Herring, *Fuel-cycle and nuclear material disposition issues associated with high-temperature gas reactors,* in *ANES 2004 Conference paper* (Miami, 2004).

[2] J. Tian, *A new ordered bed modular reactor concept,* Annals of Nuclear Energy **34**, 297 (2007).

[3] Zuoyi Zhang, Zongxin Wu, Dazhong Wang, Yuanhui Xu, Yuliang Sun, Fu Li and Yujie Dong, *Current status and technical description of Chinese 2×250MWth HTR-PM demonstration plant,* Nuclear Engineering and Design **239**, 1212 (2009).

[4] A. Koster, H.D. Matzner and D.R. Nicholsi, *PBMR design for the future,* Nuclear Engineering and Design **222**, 231 (2003).

[5] Pieter J. Venter and Mark N. Mitchell, *Integrated design approach of the Pebble Bed Modular Reactor using models,* Nuclear Engineering and Design **237**, 1341 (2007).

[6] Yanhua Zheng, Lei Shi and Yujie Dong, *Thermohydraulic transient studies of the Chinese 200 MWe HTR-PM for loss of forced cooling accidents,* Annals of Nuclear Energy **36**, 742 (2009).

[7] M. Lung and O. Gremm, *Perspectives of the thorium fuel cycle,* Nuclear Engineering and Design **180**, 133 (1998).

[8] F. Sokolov, K. Fukuda and H.P. Nawada, *Thorium fuel cycle — potential benefits and challenges,* IAEA TECDOC-1450 (2005).

[9] Andrew C. Kadak and Martin Z. Bazant, *Pebble flow experiments for pebble bed reactors,* in *2nd International Topical Meeting on High Temperature Reactor Technology*.

[10] B. Boer, J.L. Kloosterman, D. Lathouwers, T.H.J.J. van der Hagen and H. van Dam, *Optimization of a radially cooled pebble bed reactor,* Nuclear Engineering and Design **240**, 2384–2391 (2010).

[11] Brian Boer, *Optimized Core Design and Fuel Management of a Pebble-Bed Type Nuclear Reactor*, Ph.D. thesis, Delft University of Technology (2008).

[12] Yasushi Muto and Yasuyoshi Kato, *A new pebble bed core concept with low pressure drop,* in *Transactions of the Global 2003 Conference* (2003) p. 1202.

[13] Andrew C. Kadak and Martin Z. Bazant, *Improvement of fuel temperature characteristics in a pebble bed core with horizontal flow by means of fuel zoning,* in *Proceedings of ICAPP'05, Seoul, Korea* (2005).

[14] Zongxin Wu, Dengcai Lin and Daxin Zhong, *The design features of the HTR-10,* Nuclear Engineering and Design **218**, 25–32 (2002).

[15] Henri Fenech, *Heat Transfer and Fluid Flow in Nuclear Systems* (Pergamon Press, New York, 1981).

[16] Gilbert Melese and Robert Katz, *Thermal and Flow Design of Helium-Cooled Reactors* (American Nuclear Society, La Grange Park, 1984).

[17] David A. Rodriguez Sanchez, *Safety analysis of a thorium-fueled High Temperature Gas-cooled Reactor*, Master's thesis, Delft University of Technology (2012).

[18] K. Way and E. P. Wigner, *The Rate of Decay of Fission Products,* Physical Review **73**, 1318 (1948).

[19] Jens Nabaschek, *Berechningsmethoden und analysen zum dynamischen verhalten von kraftwerksanlagen mit hochtemperaturreaktor,* Ph.D. thesis, Kernforschungsanlage Jülich (1983).

[20] Bismark Mzubanzi Tyobeka, *Advanced Multi-dimensional Deterministic Transport Computational Capability for Safety Analysis of Pebble-Bed Reactors*, Ph.D. thesis, Pennsylvania State University (2007).

[21] K. Verfondern, *Experimentelle überprüfung des thermohydraulikprogramms "THERMIX" und rechnerische analyse der transienten temperature und strömungsfelder im core-bereich des THTR-reaktors nach ausfall der nachwärme abfuhr.* .

[22] Gene H. Golub and Chalres F. van Loan, *Matrix Computations* (John Hopkins University Press, London, 1996).

[23] S. Goluoglu, D. F. Hollenbach and L. M. Petrie, *CSAS6: CONTROL MODULE FOR ENHANCED CRITICALITY SAFETY ANALYSIS WITH KENO-VI*, Tech. Rep. (Oak Ridge National Laboratory, Nuclear Science and Technology Division, 2009).

[24] N. M. Greene and L. M. Petrie, *XSDRNPM: A ONE-DIMENSIONAL DISCRETE-ORDINATES CODE FOR TRANSPORT ANALYSIS*, Tech. Rep. (Oak Ridge National Laboratory, Nuclear Science and Technology Division, 2009).

[25] N. M. Greene, L. M. Petrie and S. K. Fraley, *ICE: MODULE TO MIX MULTIGROUP CROSS SECTIONS*, Tech. Rep. (Oak Ridge National Laboratory, Nuclear Science and Technology Division, 2009).

[26] B. Boer, D. Lathouwers, Ming Ding and J.L. Kloosterman, *Coupled neutronics / thermal hydraulics calculations for High Temperature Reactors with the DALTON - THERMIX code system,* in *International Conference on the Physics of Reactors, "Nuclear Power: A Sustainable Resource"* (2008).

[27] F. Reitsma, G. Strydom, J.B.M. de Haas, K. Ivanov, B. Tyobeka, R. Mphahlele, T.J. Downar, V. Seker, H.D. Gougar, D.F. Da Cruz and U.E. Sikik, *The PBMR steady-state and coupled kinetics core thermal-hydraulics benchmark test problems,* Nuclear Engineering and Design **236**, 657 (2006).

[28] F. J. Wols, J.L. Kloosterman, D. Lathouwers, T.H.J.J. van der Hagen, *Conceptual design of a passively safe thorium breeder pebble bed reactor,* (2014), submitted to Annals of Nuclear Energy.

[29] B. Boer, D. Lathouwers, J.L. Kloosterman, T.H.J.J. van der Hagen and G. Strydom, *Validation of the DALTON-THERMIX Code System with Transient Analyses of the HTR-10 and Application to the PBMR,* Nuclear Technology **170**, 306 (2010).

[30] James J. Duderstadt and Louis J. Hamilton, *Nuclear Reactor Analysis* (John Wiley & Sons, 1976).

[31] F. J. Wols, J.L. Kloosterman, D. Lathouwers, T.H.J.J. van der Hagen, *Core design and fuel management studies of a thorium-breeder pebble bed high-temperature reactor,* Nuclear Technology **186**, 1 (2014).

[32] G.J. Auwerda, J.L. Kloosterman, D. Lathouwers and T.H.J.J. van der Hagen, *Effects of random pebble distribution on the multiplication factor in HTR pebble bed reactors,* Annals of Nuclear Energy **37**, 1056 (2010).

[33] B. Boer, J.L. Kloosterman, D. Lathouwers, T.H.J.J. van der Hagen, *In-core fuel management optimization of pebble-bed reactors,* Annals of Nuclear Energy **36**, 1049 (2009).

[34] P.K. Nag, *Power Plant Engineering* (Tata McGraw-Hill, New Delhi, 2012).

[35] W. Ninaus, S. Sgouridis, F. Schürrer, H.J. Müller, K. Oswald, R.D. Neef and H. Schaal, *Investigations of an emergency shut-down system using small absorbing spheres forpebble-bed high temperature gas-cooled reactors,* in *IAEA TECDOC-1450: Gas-Cooled Reactor Safety and Accident Analysis.*

[36] J. Singh, H. Hohn and H. Barnert, *Advanced pebble bed high temperature reactor with central graphite colum for future applications,* Nuclear Engineering and Design **128**, 383 (1991).

A

SAFETY ASPECTS OF THE HTR-PM

Table A.1: Design parameters of the HTR-PM [6].

Parameters	Design value
Reactor power, MW(t)	250
Active core diameter, m	3.0
Active core height, m	11.0
Reactor pressure vessel inside diameter, mm	5700
Reactor pressure vessel thickness, mm	131
Helium pressure of primary loop, MPa	7.0
Helium mass flow rate, kg/s	96
Mean/maximum power density, MW/m3	3.22/6.57
Inlet/outlet helium temperature, °C	250/750
Number of fuel elements in equilibrium core	420,000
Metal U per fuel element, g	7
Average number of fuel element core passages	15
Average burn-up, MWd/tU	90,000

Table A.2: Temperature limits of the main components in the reactor [6].

Component	Normal operation (°C)	Accident (24 h) (°C)
RPV	350	400
Bottom supporting component	350	500
Primary circuit blower vessel	350	400
Hot gas duct	900	900
Core barrel	350	500
Reactor cavity concrete	70	100

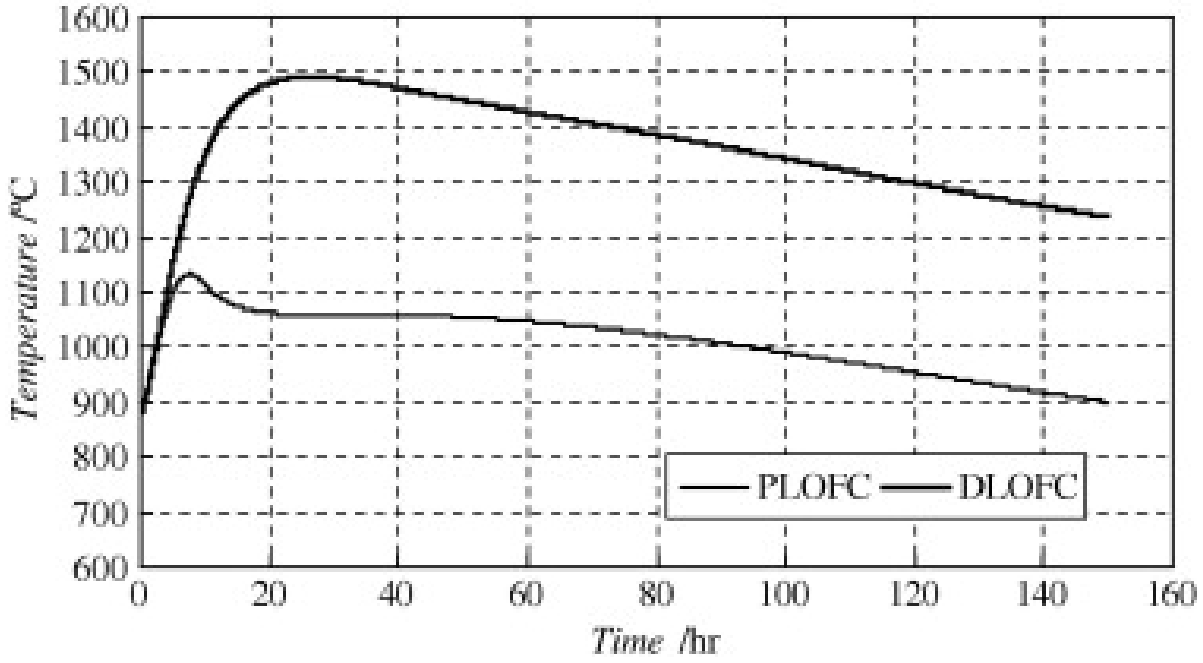

Figure A.1: Maximum fuel element temperature in the LOFC accidents of 100% rated power [6].

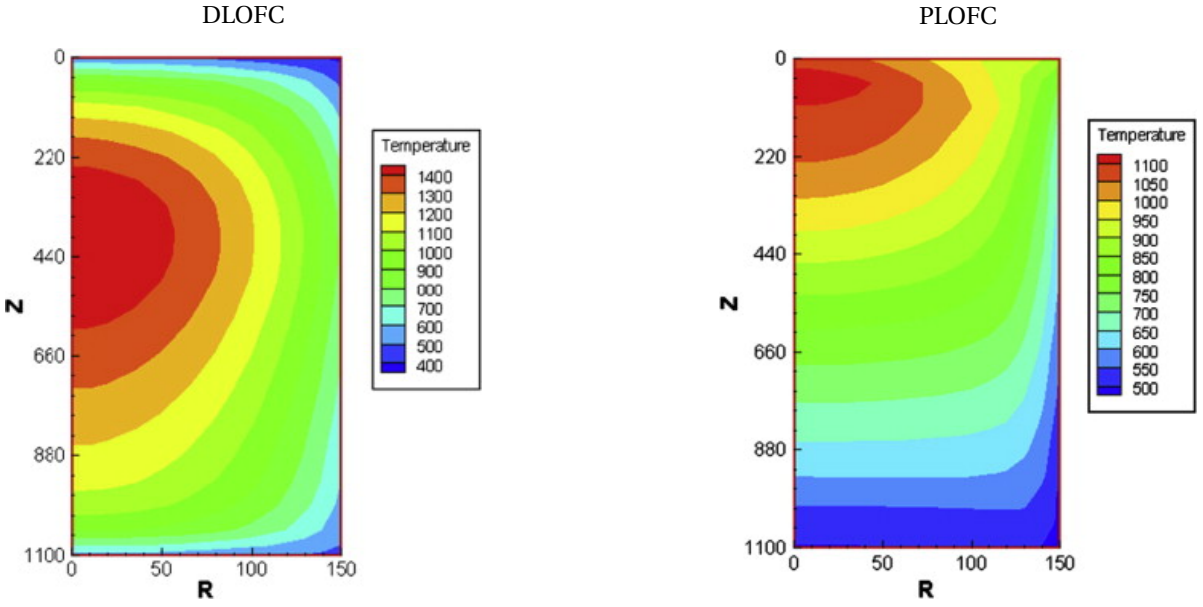

Figure A.2: Core temperature distribution in LOFC accidents of 100% rated power 26 h (°C) [6].

B

Composition input THERMIX

```
hetero 1-1 0.000e+00 0.000e+00500.0 0.000.610 3.02 0.00 00     -c09 -c01a
     6.000e+00 1.600e-02    1  7.00e+01
 2.000e+02 1.600e+03          7
 5   6.000      -c09       -c10   0.000000
 4   5.400      -c09       -c10   1.000000
 3   5.000      -c09       -c10   1.000000
 2   3.000      -c09       -c10   1.000000
 1   0.001      -c09       -c10   1.000000
topref 2 0 0.000e+00 0.000e+00200.0 0.001.000 0.00 0.00 00     -c09 -c11
botref 3 0 0.000e+00 0.000e+00200.0 0.001.000 0.00 0.00 00     -c09 -c11
sidref 4 0 0.000e+00 0.000e+00200.0 0.001.000 0.00 0.00 00     -c09 -c11
topbnd 5 1 0.000e+00 5.000e-03 70.0 0.001.000
botbnd 6 1 0.000e+00 2.000e-02 70.0 0.001.000
rbnd   7 1 0.000e+00 2.000e-02 70.0 0.001.000
inlet  8-1 0.000e+00 0.000e+00100.0 0.000.900 0.00 0.00 00     -c12 -c12
outlet 9-1 0.000e+00 0.000e+00100.0 0.000.900 0.00 0.00 00     -c12 -c12
innhor10-1 0.000e+00 0.000e+00100.0 0.000.800 0.00 0.00 00     -c09 -c11
outhor11-1 0.000e+00 0.000e+00100.0 0.000.800 0.00 0.00 00     -c09 -c11
innple12-1 0.000e+00 0.000e+00500.0 0.001.000 0.00 0.00 00     -g01 -g01
outple13-1 0.000e+00 0.000e+00700.0 0.000.400 0.00 0.00 00     -c09 -c11
innver14-1 0.000e+00 0.000e+00100.0 0.001.000 0.00 0.00 00     -g01 -g01
outver15-1 0.000e+00 0.000e+00100.0 0.000.430 0.00 0.00 00     -c09 -c11
innsli16-1 0.000e+00 0.000e+00100.0 0.000.840 0.00 0.00 00     -c09 -c11
outsli17-1 0.000e+00 0.000e+00100.0 0.000.900 0.00 0.00 00     -c09 -c11
pleria18-1 0.000e+00 0.000e+00500.0 0.000.800 0.00 0.00 00     -c09 -c11
riser 19-1 0.000e+00 0.000e+00100.0 0.000.800 0.00 0.00 00     -c09 -c11
plerib20-1 0.000e+00 0.000e+00500.0 0.000.800 0.00 0.00 00     -c09 -c11
cabrit21 0 0.000e+00 0.000e+00400.0 0.001.000 0.00 0.00 00     -c12 -c12
cabrib22 0 0.000e+00 0.000e+00400.0 0.001.000 0.00 0.00 00     -c12 -c12
cabrir23 0 0.000e+00 0.000e+00400.0 0.001.000 0.00 0.00 00     -c12 -c12
hegat 24 0 0.000e+00 0.000e+00300.0 0.001.000 0.00 0.00 00     -g01 -g01  0.90 00
hegab 25 0 0.000e+00 0.000e+00300.0 0.001.000 0.00 0.00 00     -g01 -g01  0.90 00
hegara26 0 0.000e+00 0.000e+00300.0 0.001.000 0.00 0.00 00     -g01 -g01  0.90 01
hegarb27 0 0.000e+00 0.000e+00300.0 0.001.000 0.00 0.00 00     -g01 -g01  0.90 01
insult28 0 1.000e-04 0.000e+00100.0 0.001.000 0.40 0.00 00
insulb29 0 1.000e-04 0.000e+00100.0 0.001.000 0.40 0.00 00
metint30 0 0.000e+00 0.000e+00200.0 0.001.000 0.00 0.00 00     -m01 -m01
rpv   31 0 0.000e+00 0.000e+00200.0 0.001.000 0.00 0.00 00     -m01 -m01
airgat32 0 0.000e+00 0.000e+00300.0 0.001.000 0.00 0.00 00     -g02*-g02* 0.90 00
airgab33 0 0.000e+00 0.000e+00300.0 0.001.000 0.00 0.00 00     -g02*-g02* 0.90 00
airgar34 0 0.000e+00 0.000e+00300.0 0.001.000 0.00 0.00 00     -g02*-g02* 0.90 01
```

ACKNOWLEDGEMENTS

I would like to thank...

Frank Wols first of all, for being a great supervisor with lots of expertise,

Jan-Leen Kloosterman, for his experience and useful comments to guide this project in the right direction,

Danny Lathouwers, for writing the DALTON code that was essential for my work, and for being a committee member,

Sasa Kenjeres, as member of my defence committee and for his lectures on continuum physics, which were of great help for my understanding of the transport phenomena related to this research,

Everyone of the Nuclear Energy and Radiation Applications research group, for a fantastic working environment and lots of fun during coffee and lunch breaks, especially:
Charlotte, for all collaboration on courses and the wonderful trips,
Aldo, my roommate for the last period for editing this thesis,
and the other master students Sjoerd, Wilhelm and Dick, for the (very) long walks,

All the people of student association Sint Jansbrug, for providing everything I needed outside of the study during my time as a student,

Julius Huijts for the common meal salads and late night coffee breaks during the last weeks of both our theses,

Wouter Hordijk and Jochen Hinz, for being fantastic study mates during the entire study, and for editing this thesis,

And last but certainly not least I would like to thank my father for placing my feet on the path, my sister for her enthusiasm and mad driving skills, and my mother, not only for her razor sharp grammatical comments, but for being who she is.

Joran de Jong,

26/06/2014.